

# Searching for Nambu - Goldstone Bosons at the LHC

Athanasios Dedes<sup>a</sup>, Terrance Figy<sup>b</sup>, Stefan H oche<sup>b</sup>,  
Frank Krauss<sup>b</sup>, and Thomas E. J. Underwood<sup>c</sup>

<sup>a</sup>*Division of Theoretical Physics, University of Ioannina, Ioannina, GR 45110, Greece*

<sup>b</sup>*Institute for Particle Physics Phenomenology, University of Durham, DH1 3LE, UK*

<sup>c</sup>*Max-Planck-Institut f ur Kernphysik, Saupfercheckweg 1, 69117 Heidelberg, Germany*

## ABSTRACT

Phenomenological implications of a minimal extension to the Standard Model are considered, in which a Nambu-Goldstone boson emerges from the spontaneous breaking of a global  $U(1)$  symmetry. This is felt only by a scalar field which is a singlet under all Standard Model symmetries, and possibly by neutrinos. Mixing between the Standard Model Higgs boson field and the new singlet field may lead to predominantly invisible Higgs boson decays. The “natural” region in the Higgs boson mass spectrum is determined, where this minimally extended Standard Model is a valid theory up to a high scale related with the smallness of neutrino masses. Surprisingly, this region may coincide with low visibility of *all* Higgs bosons at the LHC. Monte-Carlo simulation studies of this “nightmare” situation are performed and strategies to search for such Higgs boson to invisible (Nambu-Goldstone boson) decays are discussed. It is possible to improve the signal-to-background ratio by looking at the distribution of either the total transverse momentum of the leptons and the  $\cancel{p}_T$ , or by looking at the distribution of the azimuthal angle between the  $\cancel{p}_T$  and the momentum of the lepton pair for the  $Z$ - and Higgs-boson associated production. We also study variations of the model with non-Abelian symmetries and present approximate formulae for Higgs boson decay rates. Searching for Higgs bosons in such a scenario at the LHC would most likely be solely based on Higgs to “invisible” decays.

# 1 Introduction

In a seminal paper published in 1962, Goldstone, Salam and Weinberg [1] proved that the physical particle spectrum of a theory in which a continuous, global symmetry is spontaneously broken must contain one massless, spin-zero particle for each broken symmetry. Massless particles of this type, today called Nambu-Goldstone bosons (NGB), were first theoretically discovered in particular models by Goldstone [2] and Nambu [3]. In the following, they will collectively be denoted by the symbol  $\mathcal{J}$ . NGBs have the peculiar property that they couple to the divergence of the current  $j^\mu(x)$  associated with the symmetry that is broken. This coupling has a strength which is inversely proportional to the scale of symmetry breaking  $F$ ,

$$\mathcal{L}_{\text{int}} = \frac{1}{2F} \mathcal{J}(x) \cdot \partial_\mu j^\mu(x). \quad (1.1)$$

This form of interaction is invariant under the shift transformation,  $\mathcal{J} \rightarrow \mathcal{J} + \omega$ , where  $\omega$  is an angle that parameterizes different vacuum field configurations. Since NGBs typically are amongst the lightest particles in a theory a large fraction of the other particles can decay into them through eq. (1.1). For this decay to occur, these other particles, possibly scalars and/or quarks and leptons, must be charged under the same spontaneously broken global symmetry. It was first proposed by Suzuki and Schrock [4] that if the Standard Model (SM) Higgs boson mixes with such a new scalar particle then it must have a decay channel into a pair of NGBs ( $\mathcal{J}\mathcal{J}$ ) provided that the scale  $F$  is of the order of the electroweak gauge boson masses,  $F \approx 100$  GeV. If such a Higgs boson decay exists then it should be searched for at colliders.

The basic idea underlying this article is the existence of an additional global “phantom” symmetry,  $G_P = U(1)_P$  ( $P$  stands for “Phantom”), that is spontaneously broken at some scale  $F$ . Then following eq. (1.1),  $\mathcal{J}$  will couple to all fermions ( $f$ ) that are charged under  $G_P$  since  $\partial_\mu j^\mu = m_f \bar{f} \gamma_5 f$ . This coupling will be proportional to  $m_f/F$ . In the literature, there are three famous types of Nambu-Goldstone bosons: axions [5], familons [6] and majorons [7] and their associated broken symmetries are the Peccei-Quinn symmetry [8], and the family and lepton number symmetry, respectively. In the former two cases the global symmetry is carried by both quarks and leptons and in the latter case by leptons only. However, considerations of energy loss in stars, supernovae and/or in terrestrial collider experiments [9] conclude that  $F \gtrsim 10^{9-10}$  GeV in these popular cases. This bound constrains the decays of Higgs particles into the NGBs of the aforementioned models to be completely unobservable at colliders. Recently, a Majoron model has been considered where lepton number is spontaneously broken at the electroweak scale but in accordance

with astrophysical bounds [10], however we will not consider this class of models here. A different situation arises if we assume that such additional NGBs, if existent, must *exclusively* couple to phantom (SM gauge singlet sector) fields.

It is important to note that the requirement of renormalizability poses some constraints on such a hypothetical phantom sector. In particular, it demands that the only places where a phantom sector can make connections to the SM are the Yukawa interactions of neutrinos and Higgs bosons and the  $H^\dagger H$  “mass” term. Therefore, the only relevant phantom sector fields are a right-handed fermion (possibly coming in three copies) and (in general complex) scalar fields. This immediately triggers some thought on implications for neutrino masses. For them, there are two possibilities: Majorana or Dirac masses. The Majorana see-saw mechanism [11] in fact is nothing but a type of phantom sector. However, as already discussed, in the simplest models the possible spontaneously broken global symmetry is lepton number – clearly not a purely phantom sector symmetry. So, what about the Dirac case? Sticking to the same principle that leads to suppressed neutrino masses in the Majorana see-saw scenario, an analogous non-renormalizable operator can be constructed. It reads

$$\mathcal{L}_\nu = \frac{(\bar{L} \cdot \tilde{H})(\Phi \cdot \nu_R)}{\Lambda}. \quad (1.2)$$

In the model proposed in this article, some (purely phantom sector) symmetry  $G_P$ , prevents the interaction  $\bar{L} \cdot \tilde{H} \nu_R$  from providing neutrinos with electroweak-scale masses. Then, eq. (1.2) results in acceptably small Dirac neutrino masses after spontaneous symmetry breaking of  $G_P$  (and the extended SM gauge group  $G_{\text{SM}}$ ) at  $\langle \Phi \rangle \approx \langle \tilde{H} \rangle \approx 100$  GeV provided that  $\Lambda \sim 10^{16}$  GeV. Here, the field  $H$  (where  $\tilde{H} = i\sigma_2 H^*$ ) is the standard model  $SU(2)_L$  Higgs doublet and “ $\cdot$ ” denotes the inner product within  $G_{\text{SM}}$  or  $G_P$ . A renormalizable model resulting in the effective operator of eq. (1.2) was first built by Roncadelli and Wyler [12]. It has been recently shown in ref. [13] that this model would lead to successful baryogenesis via Dirac leptogenesis [13–15] if  $0.1 \text{ GeV} \lesssim \langle \Phi \rangle \lesssim 2 \text{ TeV}$ .

It is worth noting that this particular NGB evades many bounds applying to other species of NGB since the only fermions transforming under  $G_P$  are the  $\nu_R$ , and the coupling between the NGB and the neutrinos is proportional to  $\frac{m_\nu}{\langle \Phi \rangle} \approx \frac{\langle \tilde{H} \rangle}{\Lambda}$ . This is too small to affect neutrino flavour oscillations through  $\nu \rightarrow \nu + \mathcal{J}$  [16].

It is not unreasonable to suppose that the effects of the phantom sector may already

have been seen <sup>1</sup> in experiments revealing that neutrinos have small masses.

The existence of such a phantom sector may also be responsible for electroweak symmetry breaking. This has recently been emphasized by Patt and Wilczek [17] and also by the authors of ref. [13]. Their argument is based on the fact that no symmetry principle can forbid the mixing of the Higgs sector with the phantom sector through the renormalizable link operator

$$\mathcal{L}_{\text{link}} = \eta H^\dagger H \Phi^\dagger \Phi . \quad (1.3)$$

Eq. (1.3) suggests that the phantom sector field  $\Phi$  triggers spontaneous electroweak symmetry breaking, i.e.  $\langle H \rangle \equiv v \approx 246$  GeV once it develops a vacuum expectation value (vev),  $\langle \Phi \rangle \equiv \sigma$ . This holds true even in the absence of any tree-level Higgs mass term,  $\mu^2 H^\dagger H$  [18,19]. Furthermore, it is exactly the mixing term of eq. (1.3) that causes the Higgs boson to decay into a pair of NGBs,  $H \rightarrow \mathcal{J}\mathcal{J}$ . Since the  $\mathcal{J}$ s interact only very weakly with matter, this decay effectively constitutes an invisible decay of the Higgs boson.

Of course, this discussion could be generalized to non-Abelian groups. However, for simplicity here and onwards the simplest group  $G_P = U(1)_P$  is assumed. The Noether current associated with this symmetry is  $j_\mu(x) = i\Phi^* \overleftrightarrow{\partial}_\mu \Phi$ . The phantom field  $\Phi$  can be expanded about its vev  $\sigma$  in the usual fashion,

$$\Phi(x) = e^{i\mathcal{J}(x)/\sigma} [\sigma + \phi(x)]/\sqrt{2} . \quad (1.4)$$

Using eq. (1.1) the interaction between the massive Higgs boson  $\phi(x)$  and the NGB is found to be  $\mathcal{L}_{\text{int}} = \frac{1}{\sigma}\phi(\partial_\mu \mathcal{J})^2$ . The scalar potential is composed of the usual quadratic and quartic terms for  $H$  and  $\Phi$  as well as the link term of eq. (1.3). It is independent of  $\mathcal{J}$  i.e.  $V(H, \Phi) = V(h, \phi)$ , where  $h$  is the neutral field component of the  $SU(2)_L$ -Higgs doublet. The fields  $h = O_{i1}H_i$  and  $\phi = O_{i2}H_i$  are rotated to their physical mass eigenstates,  $H_i$ , with an orthogonal rotation matrix  $O$  (CP-conservation is assumed). After setting particles on their mass shell,  $\mathcal{L}_{\text{int}}$  becomes [4],

$$\mathcal{L}_{\text{int}} = -\frac{m_{H_i}^2}{2\sigma} O_{i2} H_i(x) \mathcal{J}(x) \mathcal{J}(x) , \quad (1.5)$$

where  $i = 1, 2$  in this minimal  $G_P = U(1)_P$  scenario<sup>2</sup>. In this case the rank-2 matrix

---

<sup>1</sup> One should also notice that, like  $\mathcal{J}$ s, the three right-handed neutrinos being SM-gauge singlets are the only light fermions that obey the shift invariance,  $\nu_R \rightarrow \nu_R + \omega$  where  $\omega$  is a Grassmann-type parameter. It may be tempting to interpret the  $\nu_R$ s as Goldstinos of an  $N_f$  (with  $n_f$  being the number of  $\nu_R$  flavours) supersymmetric phantom sector where the  $\mathcal{J}$ s belong to the same supermultiplet.

<sup>2</sup> The link term of eq. (1.3) also gives rise to quartic  $H_i H_j \mathcal{J}\mathcal{J}(i, j = 1, 2)$  couplings which are given in Fig. 11 of Appendix A. These couplings contribute to the decay,  $H_2 \rightarrow H_1 \mathcal{J}\mathcal{J}$ . However, the decay rate for this channel is on the order of  $10^{-9}$  GeV or less for benchmark scenarios considered in this paper. Hence, they will be completely neglected in the analysis presented here.

$O$  contains one mixing angle  $\theta$ . Following the notation of ref. [13], it will be fixed by  $O_{12} = -O_{21} = \sin\theta$  and  $O_{11} = O_{22} = \cos\theta$ . The limit  $\eta = 0$  implies  $\theta = 0$ , i.e. no mixing between the SM-Higgs and the phantom sector scalar fields. Obviously, in this limit the Standard Model is recovered. This article assumes a convention where  $m_{H_1} < m_{H_2}$ . Trading the vev of  $\langle\Phi\rangle \equiv \sigma$  with the more familiar  $\tan\beta \equiv v/\sigma$ , the free parameters of the model read

$$m_{H_1} \quad , \quad m_{H_2} \quad , \quad \tan\theta \quad , \quad \tan\beta \quad . \quad (1.6)$$

Eq. (1.5) is the equation underlying all phenomenological analyses in this paper. It describes Higgs boson decays to the almost sterile NGB particles. There exists an extensive body of literature, which addresses various techniques for discovering an invisible Higgs boson at colliders. They can be assembled in three main strategies:

- Studying the recoil of the  $Z$ -gauge boson in the associated  $Z + H_i$  production process. Experimental results from LEP are summarized in [20] and simulations have been performed in [21]. A study for this process at the Tevatron has been performed in refs. [22,23] with the result that the collider needs substantially more integrated luminosity to improve the current LEP exclusion limit. Parton level simulation studies for the LHC exist in Refs. [23–25]. Further hadron level/detector simulation studies for the LHC are currently under way [26,27].
- Vector boson fusion (VBF) processes. As suggested by Eboli and Zeppenfeld [28], this has now been simulated at hadron/detector level for the LHC [26,29].
- Central exclusive diffractive production has been studied for a particular model in ref. [30].

It should be noted that in all the above analyses only models with *only one* Higgs boson decaying completely invisibly were considered.

In this article the focus will be put on the first two search channels, namely  $ZH$  production and VBF. In both cases, the coupling of the Higgs to the gauge bosons is crucial. In the model considered here, only the SM-like scalar field  $h$ , belonging to the  $SU(2)_L$  Higgs-doublet, couples to vector bosons  $V$ . The corresponding SM coupling constant  $[g_{HVV}]_{\text{SM}}$  is rescaled with the mixing angle such that

$$g_{H_iVV} = O_{i1} [g_{HVV}]_{\text{SM}} \quad . \quad (1.7)$$

Since the matrix  $O$  is real and orthogonal, its elements are smaller than unity. This immediately implies that all Higgs production cross sections and/or decay rates (to SM

particles) in this model are suppressed relative to the SM by a factor  $O_{i1}^2$ . However, because of the orthogonality condition,  $\sum_i [O_{i1}]^2 = \sum_i [O_{i2}]^2 = 1$ . Therefore, if for example  $H_1$  is invisible then the other Higgs  $H_2$  tends to be visible and vice-versa. Is this a no-lose theorem for a Higgs boson discovery in this type of model? This is one of the questions to be addressed in this paper.

More specifically, in this article the following two questions will be discussed:

Q1: Is there any window in the parameter space (1.6) where LEP failed to exclude *both* Higgs-bosons for  $m_{H_i} \lesssim 114$  GeV ?

Q2: Is there any (natural) window in the parameter space (1.6) where *both* Higgs bosons would hide undetected at LHC?

In this context “natural” means that the theory has a positive definite potential, with perturbative (non-trivial) couplings up to a high cut-off scale  $\Lambda \approx 10^{16}$  GeV, where the mechanism for naturally light neutrino masses may be expected [recall eq. (1.2)]. Therefore, we begin our analysis with Section 2 where stability and triviality bounds are analyzed and plotted together with electroweak  $\rho$ -parameter constraints. In Section 3, we answer question Q1. We derive analytical formulae for the Higgs boson to “visible” ( $\mathcal{R}^2$ ) and “invisible” ( $\mathcal{T}^2$ ) decay rates and plot predictions of the model against experimental LEP exclusion data for Higgs masses less than, approximately, 114 GeV. A possible scenario explaining the LEP Higgs boson excess is also discussed in this section. In Section 4, we extend the region of validity of ( $\mathcal{R}^2$ ) and ( $\mathcal{T}^2$ ) to heavier Higgs boson masses, and justify five benchmark points. Next, in subsections 4.1-4.2, we perform a detailed Monte-Carlo simulation for signals at these points and their backgrounds, and we discuss possible strategies useful for further theoretical and experimental consideration. Furthermore, in Section 5, extensions of the Abelian to non-Abelian phantom sectors and some consequences relevant for Higgs boson phenomenology at the LHC are discussed. A discussion of our findings together with some remarks for alternative scenarios is presented in Section 7. In Appendix A, we display the relevant Feynman rules of the Abelian model.

## 2 Stability and Triviality Bounds

In the minimal phantom model, the set of physical parameters in eq. (1.6) can be written<sup>3</sup> in terms of the renormalization group running parameters  $\lambda_H H^4$ ,  $\eta H^2 \Phi^2$ , and  $\lambda_\Phi \Phi^4$ :

$$\lambda_H = \frac{1}{2} \frac{m_{H_1}^2 \cos^2 \theta + m_{H_2}^2 \sin^2 \theta}{v^2}, \quad (2.1)$$

$$\eta = \frac{1}{2} \frac{(m_{H_2}^2 - m_{H_1}^2) \sin(2\theta) \tan \beta}{v^2}, \quad (2.2)$$

$$\lambda_\Phi = \frac{1}{2} \frac{m_{H_1}^2 \sin^2 \theta + m_{H_2}^2 \cos^2 \theta}{v^2} \tan^2 \beta \quad (2.3)$$

with  $v \approx 246$  GeV. Notice that in the limit where both  $\tan \beta, \tan \theta \rightarrow 0$  the phantom sector completely decouples from the SM scalar sector. Also, note that  $\lambda_\Phi$  depends quadratically on  $\tan \beta$  and the Higgs boson masses. This implies that in the case of non-zero Higgs mixing there is always an upper bound on  $\tan \beta$  if the theory is required to remain perturbative. For example, if  $\tan \theta = 1$  and  $m_H \lesssim 200$  GeV then  $\tan \beta \lesssim 2$ . In all of our plots only the case  $\tan \beta = 1$  is considered although, as already explained, higher values of  $\tan \beta$  would further reduce the number of visible Higgs events.

There are two<sup>4</sup> classic, “theoretical” constraints on models that have been worked out numerous times in great detail for the SM and in many of its extensions [31]. Firstly, the triviality constraint is essentially the requirement that the couplings in eq. (2.1) - eq. (2.3) stay perturbative up to a certain scale  $\Lambda_T \gg v$ . Secondly, the vacuum stability constraint demands that the potential is bound from below up to a scale  $\Lambda_V \gg v$ . Applying both constraints yields  $\Lambda_T, \Lambda_V \lesssim 10^{16}$  GeV, where we recall the discussion following eq. (1.2). The vacuum stability bound can be reduced to the requirement

$$4 \lambda_H(Q) \lambda_\Phi(Q) > \eta(Q)^2, \quad (2.4)$$

at all scales  $Q \lesssim \Lambda_V$ .

The running parameters are defined at the scale  $Q_0 = M_Z$  and then evolved up to

---

<sup>3</sup>We adopt the notation of ref. [13].

<sup>4</sup>The unitarity constraint here is avoided by assuming that all quartic couplings are in a perturbative region,  $\lambda \lesssim 1$ .

higher scales with the following 1-loop renormalization group equations [32, 33]

$$\begin{aligned}
16\pi^2 \frac{d\lambda_H}{dt} &= \eta^2 + 24\lambda_H^2 + 12\lambda Y_t^2 - 6Y_t^4 - 3\lambda(3g_2^2 + g'^2) + \frac{3}{8}[2g_2^4 + (g_2^2 + g'^2)^2], \\
16\pi^2 \frac{d\eta}{dt} &= \eta \left[ 12\lambda_H + 8\lambda_\Phi - 4\eta + 6Y_t - \frac{3}{2}(3g_2^2 + g'^2) \right], \\
16\pi^2 \frac{d\lambda_\Phi}{dt} &= 2\eta^2 + 20\lambda_\Phi^2.
\end{aligned} \tag{2.5}$$

Here,  $t \equiv \ln \mathcal{Q}/\mathcal{Q}_0$ ,  $g'$  and  $g_2$  are the  $U(1)_Y$  and  $SU(2)_L$  gauge couplings, respectively, and  $Y_t$  is the top quark Yukawa coupling. We ignore all other Yukawa couplings because their effect in the running is negligible. The equations for  $Y_t$ ,  $g'$  and  $g_2$  are well known [34] and are left out for brevity. It is worth noticing that the parameter  $\eta$  is multiplicatively renormalized at one loop. Although there is no particular reason for  $\eta = 0$ , if this is the case at one energy scale then this will remain true at all energy scales.

Fig. 1 shows the light Higgs boson mass  $m_{H1}$  vs.  $m_{H2} - m_{H2}$  plane for  $\tan\beta = \tan\theta = 1$  where the background colours show the scale of new physics  $\Lambda$  required either by positivity or triviality (whichever is lower). The curved contour shows the 95% C.L. upper limit on the combined Higgs boson masses from precision electroweak data (see corresponding formula in ref. [13]). Fig. 1 should be compared with Fig. 5 of Section 4, to see the correspondence between easily accessible regions at the LHC and regions with a potentially high effective theory cut-off. The light (light green) shaded parameter region of Fig. 1 is what we will coin the *natural region* throughout this paper.

### 3 LEP searches

The LEP experiments searched first for visible Higgs boson events in the Higgsstrahlung process  $e^+e^- \rightarrow ZH$  with the Higgs boson decaying to  $b$ -quarks and leptons  $\ell$  in final state stemming from the  $Z$  boson decay. They presented [35] 95% C.L. upper limits for a parameter  $\mathcal{R}^2$  (in their notation  $S_{95}$ ), defined as the ratio of the number of Higgs boson events expected in any given model to the number expected in the Standard Model for a Higgs boson with an identical mass, as a function of the Higgs boson mass. An important point to note in this context is that  $\mathcal{R}^2$  *only* counts “visible” events. In particular, the data on decays to  $b$ -quarks will be used in the following. Then the  $\mathcal{R}^2$  parameter translates into

$$\mathcal{R}_i^2 \equiv \frac{\sigma(e^+e^- \rightarrow H_i X) \text{Br}(H_i \rightarrow YY)}{\sigma(e^+e^- \rightarrow h X) \text{Br}(h \rightarrow YY)}, \tag{3.1}$$

where  $i = 1, 2$ ,  $X$  are the remnants associated with the production of a  $H_i$  or  $h$  (the SM Higgs boson) and  $YY$  could be in principle either  $b\bar{b}$ , or  $\tau\tau$ , but *not*  $\mathcal{J}\mathcal{J}$ . However, in the

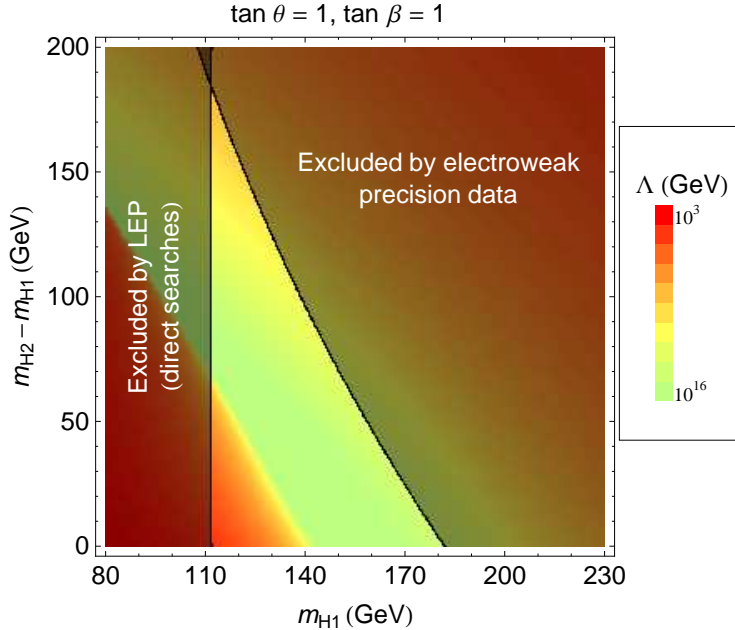


Figure 1: The light Higgs boson mass  $m_{H_1}$  vs.  $m_{H_2} - m_{H_1}$  plane for  $\tan \beta = \tan \theta = 1$ , showing the expected cut-off  $\Lambda$  of the effective theory taking the triviality and positivity of the potential into account (the lower of either  $\Lambda_T$  or  $\Lambda_V$  is shown). The curved line shows the 95% C.L. upper limit on the Higgs boson masses stemming from precision electroweak data.

framework of the particular model studied here, another possibility is that  $YY = H_j H_j$ . Exclusion limits in this case have been presented in [35].

The four LEP experiments [36] also performed searches for acoplanar jets (as signal for  $Z(\rightarrow q\bar{q}) H(\rightarrow \text{invisible})$  or leptons (as signal for  $Z(\rightarrow \ell\ell) H(\rightarrow \text{invisible})$ , with  $\ell = e, \mu$ , apart from the DELPHI-collaboarion which also used  $\tau$ 's in the final state. In all cases, the emergence of invisible decay products of the Higgs boson is identified with the production of missing energy ( $\cancel{E}$ ). Their study resulted in an upper limit on the branching ratio of  $H \rightarrow \text{invisible}$  as a function of the Higgs mass, multiplied by the production cross-section normalized to the rate expected from a SM Higgs decaying completely invisibly. In our case, this limit places constraints on the parameter

$$\mathcal{T}_i^2 \equiv \frac{\sigma(e^+e^- \rightarrow H_i X)}{\sigma(e^+e^- \rightarrow h X)} \text{Br}(H_i \rightarrow \mathcal{J}\mathcal{J}), \quad (3.2)$$

where again  $i = 1, 2$ ,  $h$  is the SM Higgs boson and  $X$  are the remnants associated with the production of  $H_i$  or  $h$  at LEP.

A further important constraint comes from the OPAL collaboration who performed a model-independent analysis of the Higgs sector at LEP [37]. They searched for the generic process  $e^+e^- \rightarrow ZS^0$  where  $S^0$  is a completely neutral (and hence invisible) scalar boson. Since this analysis is independent of the eventual fate of the Higgs candidate it bounds the parameter

$$s_i^2 \equiv \frac{\sigma(e^+e^- \rightarrow ZH_i)}{\sigma(e^+e^- \rightarrow Zh)}, \quad (3.3)$$

as a function of the Higgs boson mass. In this model  $s_1 = \cos^2 \theta$  and  $s_2 = \sin^2 \theta$ .

Particularly simple expressions may be derived for  $\mathcal{R}_i^2$  and  $\mathcal{T}_i^2$  in the minimal phantom scenario provided that the narrow width approximation may be assumed and that the Higgs boson to off-shell gauge boson decay modes may be neglected. Our analytical findings closely follow the model-independent analysis of ref. [38]. Consider the case where  $YY = b\bar{b}$  in eq. (3.1). For simplicity let us assume that the decay  $H_2 \rightarrow H_1H_1$  is kinematically forbidden, i.e.  $m_{H_1} > m_{H_2}/2$ . In this case  $\text{Br}(H_i \rightarrow b\bar{b}) + \text{Br}(H_i \rightarrow \mathcal{J}\mathcal{J}) \approx 1$ . Applying this to eq. (3.1) in the LEP search region,  $m_{H_2}/2 < m_{H_1} \lesssim 115$  GeV and after some algebra we arrive at

$$\begin{aligned} \mathcal{R}_1^2 &\simeq \left[ (1 + \tan^2 \theta) \left( 1 + \frac{1}{12} \frac{m_{H_1}^2}{m_b^2} \tan^2 \theta \tan^2 \beta \right) \right]^{-1}, \\ \mathcal{R}_2^2 &\simeq \left[ (1 + \cot^2 \theta) \left( 1 + \frac{1}{12} \frac{m_{H_2}^2}{m_b^2} \cot^2 \theta \tan^2 \beta \right) \right]^{-1}. \end{aligned}$$

Firstly, notice that the number of Higgs boson events where the Higgs boson decays to  $b\bar{b}$  (or indeed any other visible mode) are always suppressed relative to the SM prediction in which  $\text{Br}(h \rightarrow b\bar{b}) \approx 1$  for this particular Higgs boson mass region. Secondly, the number of visible Higgs boson events decreases in the limit  $m_{H_i} \gg m_b$ . Note also that if  $\tan \beta > 1$ ,  $\mathcal{R}_i^2$  receives an additional suppression.

The importance of the Higgs boson to invisible decay and of model-independent Higgs boson analyses are highlighted when we consider the example  $\tan \theta = 1$  and  $\tan \beta = 2$  where we obtain  $\mathcal{R}_i^2 = 0.012$  for  $m_{H_i} = 50$  GeV. In principle, this is within the region allowed by LEP “visible” Higgs search data [35] which excludes  $0.015 \lesssim \mathcal{R}_i^2 \lesssim 0.2$  for Higgs masses in the range  $12 \text{ GeV} \lesssim m_{H_i} \lesssim 100 \text{ GeV}$ .

This could have been a “nightmare” scenario; LEP would have completely missed the Higgs sector! Fortunately, this nightmare is averted by both the LEP Higgs boson to invisible searches and the OPAL model-independent Higgs boson search, because the former, for

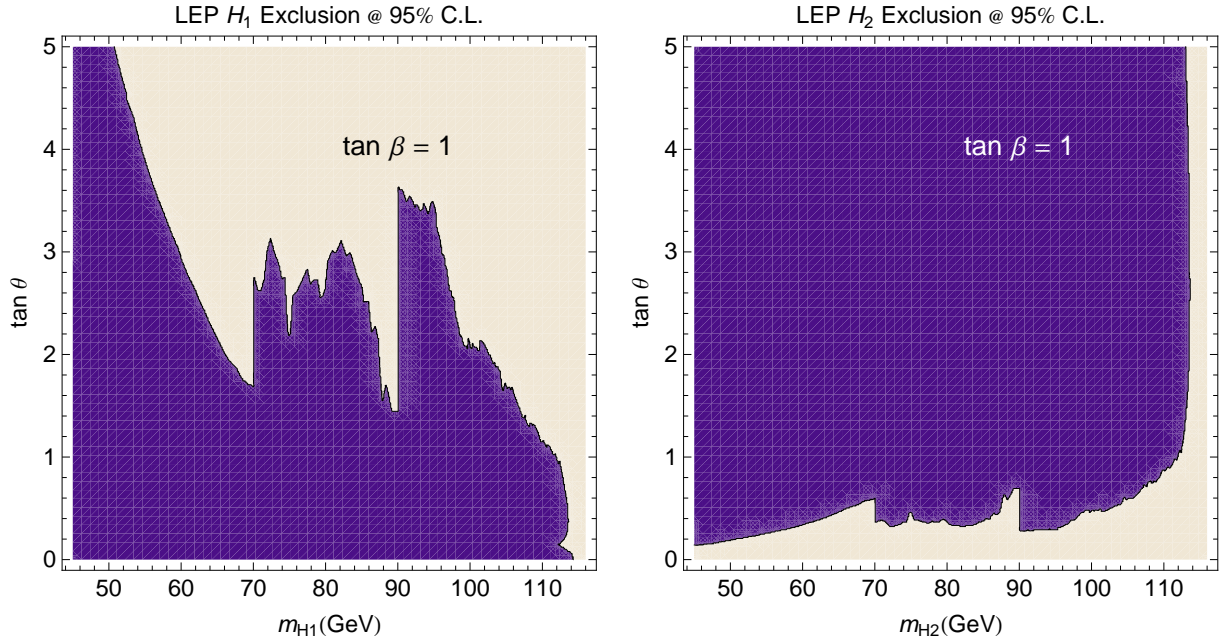


Figure 2: LEP excluded regions (at 95 % C.L.) (in dark blue) for  $\tan \theta$  versus Higgs boson masses  $m_{H_1}$  (left plot) and  $m_{H_2}$  (right plot) for the minimal phantom scenario with  $\tan \beta = 1$ . Both searches are clearly complementary to each another in this scenario.

instance, sets bounds on  $\mathcal{T}_i^2$ . In the relevant LEP mass region,  $m_{H_2}/2 < m_{H_1} \lesssim 115$  GeV,

$$\mathcal{T}_1^2 = \cos^2 \theta - R_1^2, \quad (3.4)$$

$$\mathcal{T}_2^2 = \sin^2 \theta - R_2^2. \quad (3.5)$$

Setting  $R_i^2 \rightarrow 0$  implies that  $\mathcal{T}_1^2 + \mathcal{T}_2^2 \approx 1$ . LEP searches for invisible Higgs bosons exclude  $\mathcal{T}_i^2 \gtrsim 0.5$  for masses below 110 GeV,  $m_{H_i} \lesssim 110$  GeV. Therefore, *it is unlikely that there are two invisible Higgs bosons in the LEP search region with masses  $m_{H_i} \lesssim 110$  GeV.* This answers question Q1 posed in the introduction.

In addition, using the model-independent analysis of OPAL [37],  $m_{H_i} \lesssim 85$  GeV is excluded for  $s_i^2 > 0.5$ . Since either  $s_1^2 = \cos^2 \theta \geq 0.5$  or  $s_2^2 = \sin^2 \theta \geq 0.5$  for any given  $\theta$ , *OPAL excludes the case where both  $m_{H_1} \lesssim 85$  GeV and  $m_{H_2} \lesssim 85$  GeV, independently of how the Higgs bosons actually decay.*

It is interesting to note that one Higgs boson could still be hidden in the LEP search region even with these strong constraints, while the other Higgs boson then would wait for its discovery in the allowed region out of reach of LEP.

The results of a detailed analysis of this model, including visible, invisible and model-independent LEP bounds [35–37] are summarised in Fig. 2. This numerical analysis confirms the analytical findings above. With  $\tan \beta = 1$ , a light Higgs boson ( $H_1$ ) with a mass as low as 65 GeV could have escaped unobserved at LEP if  $\tan \theta \gtrsim 2$ . For the same range of  $\tan \theta$  the other Higgs ( $H_2$ ) is constrained to be heavier than 114 GeV. From inspection of Fig. 2 we can define a LEP-allowed benchmark scenario B1 for the phantom model presented here, namely:

$$\begin{aligned} \text{B1 : } \quad m_{H_1} = 68 \text{ GeV} \quad , \quad m_{H_2} = 114 \text{ GeV} \quad , \\ \tan \theta = 2 \quad , \quad \tan \beta = 1 . \end{aligned} \tag{3.6}$$

In this case one Higgs boson is buried, undiscovered in the LEP search region (with  $\mathcal{R}_1^2 \rightarrow 0$  and  $\mathcal{T}_1^2 \rightarrow 0$ ) and the other heavier Higgs has  $\mathcal{R}_2^2 = 0.06$  and  $\mathcal{T}_2^2 = 0.74$ . With this set of parameters, very few  $H_2$  events are SM-like decays into “visible” final states and instead  $H_2$  decays mainly into “invisible” NGBs. This scenario could well be classed as a (LEP) nightmare!

### 3.1 A digression : 2.3 $\sigma$ LEP Higgs search excess

The LEP experiments established a small,  $2.3\sigma$  effect in their Higgs boson searches corresponding to a Higgs boson mass of about 98 GeV [39]. Explaining this excess would require a value of  $\mathcal{R}_1^2 \simeq 0.2$ , ruling out a Standard Model Higgs boson as plausible explanation. It is possible to provide a candidate Higgs boson in the phantom model discussed in this publication, which would have produced such an effect in the LEP data. Fig. 3 shows the allowed region in the  $\tan \theta$  vs.  $\tan \beta$  plane for  $m_{H_1} = 98$  GeV. The allowed region is tightly constrained because of the searches for invisible Higgs bosons at LEP in this mass region. At the relatively small values of  $\tan \beta$  still allowed, the main reason for such a small value of  $\mathcal{R}_1^2$  is Higgs mixing rather than the extra invisible decay mode suppressing the Higgs branching ratio.

Fig. 4 shows the constraints on this region of parameter space coming from considering the triviality and positivity of the potential. For a suitably heavy  $m_{H_2} \gtrsim 210$  GeV, most of the region suggested by the LEP excess is described by a theory which could be valid to scales as high as  $10^{16}$  GeV. When  $\tan \theta \sim 1$ , as  $\tan \beta \rightarrow 0$  ( $\sigma \rightarrow \infty$ ) the values of  $\eta$  and  $\lambda_\Phi$  tend to 0. Higgs masses around the electroweak scale are maintained in this limit because  $\mu_H^2 \rightarrow \infty$  whilst  $\mu_\Phi^2 \sim -v^2$ .

Note that the second Higgs boson mass is restricted by the upper limit on Higgs boson masses from precision electroweak data [13], however for  $m_{H_2} \lesssim 210$  GeV the whole region

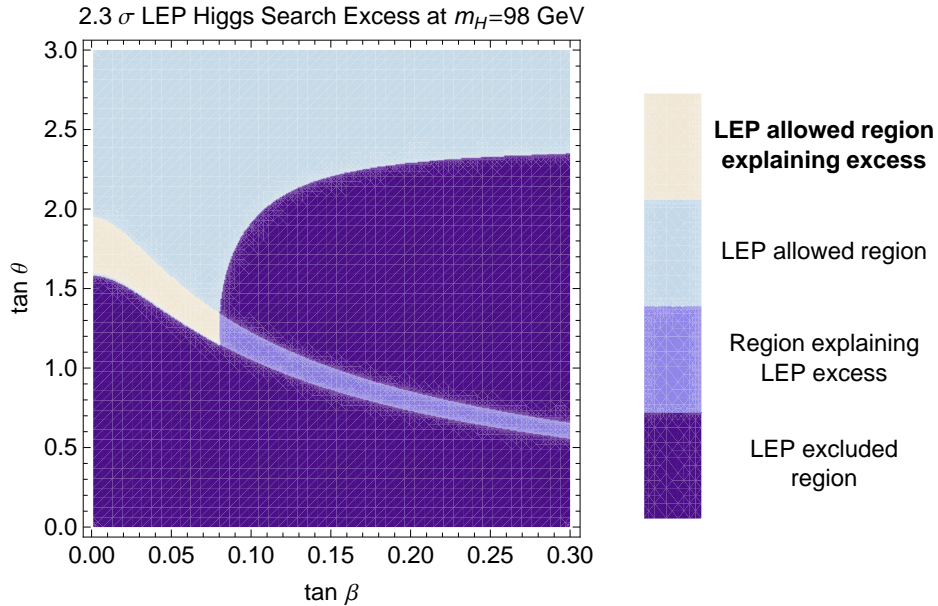


Figure 3: The  $\tan \theta$  vs.  $\tan \beta$  plane for a lightest Higgs mass of 98 GeV. The lightest region indicates where the  $2.3\sigma$  effect in the LEP Higgs searches could be explained whilst still being consistent with other LEP Higgs search data (such as the search for invisible Higgs bosons).

suggested by the LEP excess is free from this constraint. Clearly further data would be required before this effect could be taken more seriously.

In the next chapter we will address the question of whether the LHC has the sensitivity required to discover these scenarios, in particular the potential nightmare B1. The possible existence of other challenging scenarios with heavier Higgs bosons will also be examined.

## 4 LHC : expectations and strategic searches

In the LHC search region, the parameters  $\mathcal{R}_i^2$  and  $\mathcal{T}_i^2$  can be defined by expressions similar to those in eqs. (3.1) and (3.2), respectively, with the obvious replacement of the electron/positron initial state to a proton/proton initial state and  $YY = \gamma\gamma, b\bar{b}, VV, gg$ , etc.. Two categories for the ratios  $\mathcal{R}_i^2$  may be distinguished: (a) a region where  $m_{H_i} < 2m_V$  and  $H_i$  decays dominantly into  $b\bar{b}$  and (b) a region where  $m_{H_i} \gtrsim 2m_V$  and the  $H_i$  decays dominantly into a gauge boson pair,  $VV$ , with  $V = Z, W$ .

In case (a), and under the assumption that gauge bosons are produced on-shell, analytical approximations for  $\mathcal{R}_i^2$  are identical to those studied in the previous chapter. On

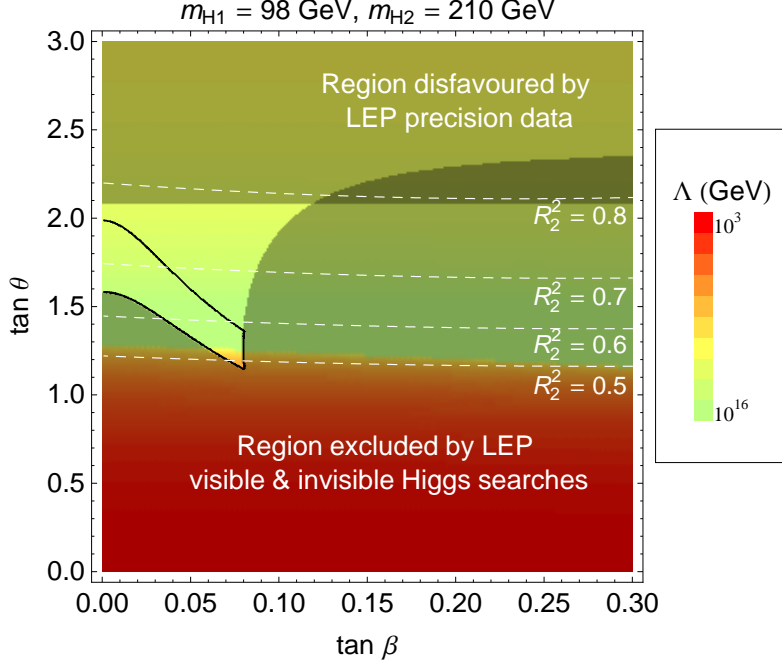


Figure 4: The  $\tan \theta$  vs.  $\tan \beta$  plane for Higgs boson masses of  $m_{H1} = 98$  GeV and  $m_{H2} = 210$  GeV. The region enclosed by the black line indicates where the  $2.3\sigma$  effect in the LEP Higgs searches could be explained whilst still being consistent with other LEP data for Higgs boson searches. The background colors indicate the scale of the expected cut-off  $\Lambda$ , of the effective theory taking the triviality and positivity of the potential into account. Darkly shaded regions are excluded by LEP Higgs search data. Contours for  $\mathcal{R}_2^2$  are shown in white.

the other hand, assuming a common gauge boson mass  $m_V$ , in region (b), we obtain

$$\mathcal{R}_1^2 \simeq \left[ (1 + \tan^2 \theta) \left( 1 + \frac{1}{3g(x_1)} \tan^2 \theta \tan^2 \beta \right) \right]^{-1},$$

$$\mathcal{R}_2^2 \simeq \left[ (1 + \cot^2 \theta) \left( 1 + \frac{1}{3g(x_2)} \cot^2 \theta \tan^2 \beta + \frac{f(y)}{g(x_2)} \frac{\cot^2 \theta}{(1 + \cot^2 \theta)^2} (\cot \theta - \tan \beta)^2 \right) \right]^{-1},$$
(4.7)

where  $x_i = m_V^2/m_{Hi}^2$ , and  $g(x) = (1 - 4x + 12x^2)(1 - 4x)^{1/2}$ . The last term in eq. (4.7) is the contribution from the heavy Higgs boson decay  $H_2 \rightarrow H_1 H_1$  [33, 40]. Furthermore,  $y = m_{H1}^2/m_{H2}^2$  and  $f(y) = (1 + 4y + 4y^2)(1 - 4y)^{1/2} \Theta(1 - 4y)$ . Imposing some constraints

to this analysis (see section 2), the mode  $H_2 \rightarrow H_1 H_1$  will not be important in further discussions.

It is apparent from eq. (4.7) that a certain suppression of the observable rates ( $\mathcal{R}_i^2$ ) is always present. Its origin is twofold. Firstly, the couplings between the  $H_i$  and SM fields are always suppressed because of the mixing matrix  $O$ . Secondly, the decay widths of the Higgs bosons are enhanced by the extra decay mode  $H_i \rightarrow \mathcal{J}\mathcal{J}$ . The contribution of this additional decay mode is increased at large  $\tan\beta$  and for  $\tan\beta = 10$  and  $\tan\theta = 1$  the suppression of visible events is always more than 90% for  $m_{H_2} \lesssim 200$  GeV. However, as we have already remarked in section 2, high values of  $\tan\beta$  result in non-perturbative couplings and will therefore not be considered in this article.

What then would be a nightmare scenario for the LHC? At present both the ATLAS and CMS collaborations have performed studies, at detector simulation level, to explore the discovery potential of their apparatus for both SM-like Higgs bosons which decay to visible final states, see e.g. [41], and Higgs bosons decaying to invisible final states, for example [27, 29]. These studies are sensitive to the ratios  $\mathcal{R}_i^2$  and  $\mathcal{T}_i^2$  as functions of the Higgs boson mass. For example, looking at the simulation results for the LHC with  $\mathcal{L} = 10(30)$  fb $^{-1}$  integrated luminosity we estimate (with naïve scaling) that it would be difficult to discover a visibly-decaying Higgs if signal event rates were 30%(20%) of that expected in the SM ( $\mathcal{R}_i^2 \lesssim 0.3(0.2)$ ). Furthermore, studies of the sensitivity of the ATLAS detector<sup>5</sup> to invisibly decaying Higgs bosons suggest that after  $\mathcal{L} = 10(30)$  fb $^{-1}$  integrated luminosity ATLAS could exclude Higgs bosons with  $\mathcal{T}_i^2 \gtrsim 0.30(0.25)$  at 95% C.L. [27, 29].

To further illustrate the necessity of the Higgs boson to invisible searches in this minimal phantom scenario, in Fig. 5 areas on the  $m_{H_1}$  vs.  $m_{H_2} - m_{H_1}$  plane are plotted where  $\mathcal{R}_i^2 \geq 0.3$  and/or  $\mathcal{T}_i^2 \geq 0.3$ . These limits define naïve regions, where Higgs bosons will experimentally be accessible at the LHC, either in visible or invisible search channels. Clearly at this stage in this study these limits are assumptions, and in fact the true experimental reach of the LHC will not be known until after it has been running for some time and predictions for the levels of backgrounds have been confirmed (or not). These assumptions do, however, serve as a good first estimate on which to justify the further study undertaken here.

In producing Fig. 5 all Higgs boson decay modes including decays to off-shell vector bosons have been considered. Different colours indicate regions where either one, both or no Higgs bosons can be seen in different channels. It is clear that a truly challenging region for LHC region remains where  $\mathcal{R}_i^2 \leq 0.3$  and  $\mathcal{T}_i^2 \leq 0.3$ . This motivates the further

---

<sup>5</sup>Similar studies exist for the CMS detector [42].

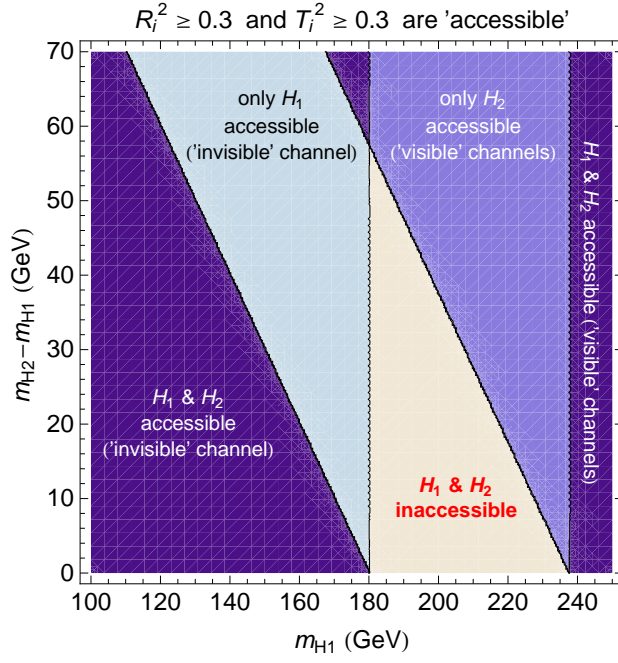


Figure 5: Regions in the  $m_{H_1}$  vs.  $m_{H_2} - m_{H_1}$  plane for  $\tan \beta = 1$  and  $\tan \theta = 1$ , where different Higgs bosons are “accessible” at LHC. We define that a given  $H_i$  is accessible if either  $\mathcal{R}_i^2 \geq 0.3$  or  $\mathcal{T}_i^2 \geq 0.3$ . In the dark (blue) regions both Higgs bosons are accessible. In the white (beige) region no Higgs bosons are accessible.

more detailed Monte Carlo analysis in the later sections of this article, which probe more carefully the possibility of discovering a Higgs boson in the invisible search channel when  $\mathcal{T}_i^2 \lesssim 0.3$ .

Using equations (3.4) and (3.5) it is easy to see that  $\mathcal{R}_1^2 + \mathcal{R}_2^2 + \mathcal{T}_1^2 + \mathcal{T}_2^2 = 1$ . The following no-lose theorem then exists: If experiments can discover a Higgs boson over the whole range of  $\mathcal{R}_i^2$  down to  $\mathcal{R}_i^2 = 0.25$  or over the whole range of  $\mathcal{T}_i^2$  down to  $\mathcal{T}_i^2 = 0.25$  then at least one Higgs boson should be found.

Without real data, estimates of the capabilities of experiments like ATLAS and CMS may easily be too optimistic or too pessimistic. Therefore in this publication, a constructive approach is taken. The phantom model has been added to the Monte Carlo event generator SHERPA [43], ready to be used when real data arrive. For now Fig. 5 may be used to define additional benchmark scenarios, some in potentially nightmarish regions, and these points can be studied in more detail. The particular scenarios are displayed in Table 1.

The LO branching ratios for both Higgs bosons are presented in Table 2. These ratios are in agreement with the analytical LO expressions in eq. (4.7) and Fig. 5, and the discussion following them. The most optimistic benchmark point is B1 and the most challenging one is B5.

$\tan \theta = 1 \quad \tan \beta = 1$		
Benchmark	$m_{H_1}(\text{GeV})$	$m_{H_2}(\text{GeV})$
B2	112	130
B3	140	165
B4	160	190
B5	185	190

Table 1: Four LHC benchmark scenarios for the phantom model.

Benchmark	Higgs	$\Gamma_{tot}(\text{GeV})$	$b\bar{b}$	$W^+W^-$	$ZZ$	$\mathcal{J}\mathcal{J}$
B1	$H_1$	0.041	0.694	–	–	99.222
	$H_2$	0.051	3.567	0.289	0.020	95.533
B2	$H_1$	0.117	0.958	0.059	0.003	98.823
	$H_2$	0.183	0.697	0.348	0.042	98.784
B3	$H_1$	0.229	0.593	0.779	0.103	98.408
	$H_2$	0.490	0.319	23.769	0.498	75.339
B4	$H_1$	0.387	0.393	12.217	0.396	86.904
	$H_2$	1.066	0.166	36.597	10.313	52.879
B5	$H_1$	0.921	0.188	36.500	6.787	56.475
	$H_2$	1.066	0.166	36.597	10.31	52.879

Table 2: Branching ratios (in percent) and total widths (in units of GeV) for the Higgs bosons,  $H_i(i = 1, 2)$ , for the benchmark points of Table 1. Branching ratios that are not displayed, account for less than 0.4%.

Prospects for discovering the Higgs bosons in the various benchmark scenarios B1-B5 at the LHC will be studied in the following. Theoretical vacuum stability and triviality bounds as well as bounds from fitting electroweak (EW) observables have already been presented in Section 2. All benchmark scenarios selected in Table 1 satisfy the EW constraints and in some the effective theory may be valid even to scales as high as the Planck scale.

## 4.1 $ZH$ -production

The first search channel for an invisibly decaying Higgs boson at the LHC considered here is the associated production of a  $Z$  and a Higgs boson, where the  $Z$  decays leptonically. This ensures that a corresponding event can be triggered. The backgrounds to this process include  $ZZ$ ,  $WW$ ,  $WZ$  and  $Z$  production with corresponding decays, and fully leptonic  $t\bar{t}$

production<sup>6</sup>. It should be noted here that in principle some information on the rates can be obtained directly from data: for  $ZZ$  pairs, final states with four leptons may be reweighted with the corresponding  $Z \rightarrow \nu\bar{\nu}$  branching ratio, in the  $WW$  case, different sign, different lepton pairs may be invoked. For the  $WZ$  background, it may be possible to extrapolate from events where three leptons are seen to those where one lepton is lost, i.e. either outside the detector acceptance or undetected. For top-pair production, semi-leptonic events may help.

All processes have been simulated with SHERPA [43] in the following setup: In order to correctly model hard parton radiation SHERPA employs the multijet matrix element-parton shower merging procedure of [44]. Therefore, for all processes discussed here and in the next section, matrix elements with at least one and in most cases two additional jets have been added to the simulation. This ensures that the simulation correctly describes the important high- $p_{\perp}$  tails of various distributions. However, all cross sections quoted are, in principle, obtained at leading-order accuracy, with no  $K$ -factors added to them. CTEQ6L parton distribution functions are used with  $\alpha_s(M_Z) = 0.118$  [45].  $\alpha_s$  is computed at two-loop accuracy. All scales are set according to the merging prescription of [44]. Jets have been defined in all cases through the  $k_T$  algorithm [46]. The CKM matrix has been chosen to be diagonal.

We have simulated and analysed events with electrons in the final state; mostly identical numbers would have been obtained if we had specialised for muon pairs instead. Obviously, this difference would be of great importance if detector effects had been included as well<sup>7</sup>. However it should suffice to state that we quote final results for leptons  $\ell = e, \mu$ . We also omitted all effects due to the underlying event because of the large uncertainties related to its modelling and the rather small impact it has on the observables we discuss.

The selection cuts listed in Ref. [27] have been applied. Thus we require:

1. one lepton pair of the same kind with opposite charges, where each lepton individually satisfies  $p_{T,\ell} > 15$  GeV and  $|\eta_{\ell}| < 2.5$ ;
2.  $|M_{\ell\bar{\ell}} - M_Z| \leq 10$  GeV;
3.  $\cancel{E}_T > 100$  GeV;
4. a veto on jets with  $p_T > 20$  GeV,  $|\eta| < 4.9$ ;

---

<sup>6</sup> Note that, in all processes, off-shell effects,  $Z$ - $\gamma$  interference etc. are fully included in the simulation.

<sup>7</sup> We refrained from including full detector simulations, or any Gaussian smearing or electron-jet conversion “by hand” and concentrated on an analysis at the hadron level, including all effects of fragmentation, hadron decays, final state QED bremsstrahlung etc..

	$ZZ$	$W^\pm Z$	$W^+W^-$	$t\bar{t}$	$Z$
$\sigma_{\text{tot}}^{\text{gen}}$ [fb]	164	$1.17 \cdot 10^3$	$1.01 \cdot 10^4$	$7.44 \cdot 10^4$	$1.81 \cdot 10^6$
$\ell^+\ell^-$ only	$2.00 \cdot 10^{-1}$	$1.10 \cdot 10^{-1}$	$6.59 \cdot 10^{-2}$	$8.40 \cdot 10^{-2}$	$1.41 \cdot 10^{-1}$
$ m_{\ell\ell} - M_Z  < 10$ GeV	$1.87 \cdot 10^{-1}$	$9.17 \cdot 10^{-2}$	$8.92 \cdot 10^{-3}$	$1.09 \cdot 10^{-2}$	$1.25 \cdot 10^{-1}$
$\cancel{E}_T > 100$ GeV	$3.69 \cdot 10^{-2}$	$1.10 \cdot 10^{-2}$	$5.91 \cdot 10^{-4}$	$2.41 \cdot 10^{-3}$	$1.94 \cdot 10^{-7}$
jet veto	$1.64 \cdot 10^{-2}$	$2.13 \cdot 10^{-3}$	$3.53 \cdot 10^{-5}$	$2.00 \cdot 10^{-6}$	-
$m_T > 200$ GeV	$1.54 \cdot 10^{-2}$	$1.95 \cdot 10^{-3}$	$2.74 \cdot 10^{-5}$	$1.19 \cdot 10^{-9}$	-
$\Delta R_{\ell\ell} < 1.75, p_T(\ell\ell, \cancel{E}_T) < 60$ GeV	$1.23 \cdot 10^{-2}$	$1.50 \cdot 10^{-3}$	$2.23 \cdot 10^{-9}$	$1.55 \cdot 10^{-10}$	-
$\sigma_{\text{eff}}$ [fb]	2.02	1.75	$2.25 \cdot 10^{-5}$	$1.15 \cdot 10^{-5}$	-

Table 3: Generation characteristics for the background processes to the  $ZH$ -channel. In all cases we included all leptonic decay modes: In the  $ZZ$  case, therefore the final state included a lepton and a neutrino pair, in the  $WZ$  case, we included a lepton pair from the  $Z$  and a lepton-neutrino pair from the  $W$ , the  $WW$  channel was supposed to decay fully leptonically in all possible combinations, for the top pairs we assumed purely leptonic decays, and for the  $Z$  a leptonic final state (no neutrinos) was demanded.

5. a veto on b-jets with  $p_T > 15$  GeV,  $|\eta| < 4.9$ ;
6.  $m_T > 200$  GeV, where  $m_T = \sqrt{2p_T^{\ell\bar{\ell}}p_T(1 - \cos\phi)}$ .

Additionally, we impose :

6.  $\Delta R_{\ell\bar{\ell}} < 1.75$ ;
7.  $p_T(\ell\bar{\ell}\cancel{E}_T) < 60$  GeV.

For the various backgrounds listed above, cross sections before and after these additional selection cuts are listed in Table 3. Generation cross sections, selection cut efficiencies and the resulting selection cross sections for the signal in the different benchmark scenarios are given in Table 4. It should be stressed again that all cross sections quoted have been obtained at leading order accuracy.

The numbers from both Tables 3 and 4 suggest that the two most dangerous backgrounds to the  $ZH$  signal are  $ZZ$  and  $WZ$  production, with corresponding decays. Following our discussion above, however, it seems that the total cross sections and distributions related to these backgrounds can be directly extracted from data in the  $ZZ$  case or

	$B_1$	$B_2$	$B_3$	$B_4$	$B_5$
$\sigma_{\text{tot}}$ [fb]	280	114.6	53.0	29.0	13.6
$\ell^+\ell^-$ only	$1.75 \cdot 10^{-1}$	$1.98 \cdot 10^{-1}$	$2.25 \cdot 10^{-1}$	$2.40 \cdot 10^{-1}$	$2.24 \cdot 10^{-1}$
$ m_{\ell\ell} - M_Z  < 10$ GeV	$1.62 \cdot 10^{-1}$	$1.84 \cdot 10^{-1}$	$2.10 \cdot 10^{-1}$	$2.23 \cdot 10^{-1}$	$2.08 \cdot 10^{-1}$
$\cancel{E}_T > 100$ GeV	$3.12 \cdot 10^{-2}$	$6.07 \cdot 10^{-2}$	$8.91 \cdot 10^{-2}$	$1.08 \cdot 10^{-1}$	$1.12 \cdot 10^{-1}$
jet veto	$3.00 \cdot 10^{-2}$	$5.66 \cdot 10^{-2}$	$7.85 \cdot 10^{-2}$	$9.29 \cdot 10^{-2}$	$1.08 \cdot 10^{-1}$
$m_T > 200$ GeV	$2.88 \cdot 10^{-2}$	$5.49 \cdot 10^{-2}$	$7.64 \cdot 10^{-2}$	$9.08 \cdot 10^{-2}$	$1.06 \cdot 10^{-1}$
$\Delta R_{\ell\ell} < 1.75, p_T(\ell\ell, \cancel{E}_T) < 60$ GeV	$2.55 \cdot 10^{-2}$	$4.93 \cdot 10^{-2}$	$6.94 \cdot 10^{-2}$	$8.35 \cdot 10^{-2}$	$9.85 \cdot 10^{-2}$
$\sigma_{\text{eff}}$ [fb]	7.15	5.65	3.68	2.42	1.34

Table 4: Generation characteristics for the signal processes in the  $ZH$ -channel.

In each case we assumed all leptonic decay channels for the  $Z$  boson.

probably well extrapolated from measurements. After cuts we find that the backgrounds together account for roughly 8 fb, leaving us with signal-to-background ratios of the order of  $S/B \approx 1/8$  up to 1. We therefore conclude that it should be possible to find the signal in all five benchmark scenarios. However, we would like to stress here that more conclusive numbers can be obtained after a simulation at detector level only.

Such detector-level studies for an invisibly decaying Higgs boson have been for the ATLAS experiment [27] found signal-to-background ratios reaching up to 1/4. Although this is of the same order of magnitude as our results, there are several differences: First of all, in our simulation the SHERPA Monte Carlo event generator with multijet merging was used for both signal and background events, while the ATLAS study employed the PYTHIA [47] event generator for the backgrounds and the program h2hv [48] for the signal. While SHERPA and PYTHIA are formally of the same accuracy there are a number of differences, like SHERPA multijet merging leading to an improved treatment of hard QCD radiation, and the full inclusion of spin correlations in SHERPA, which are not present in PYTHIA. This may have lead to a better separation of signal and background in SHERPA. On the other hand, in ATLAS' simulation the  $HVV$  couplings where assumed to have exactly the same strength as in the SM - which is not true for our analysis, where these couplings are reduced due to mixing effects. In addition, a 100% branching ratio of Higgs boson to invisible was assumed for the ATLAS simulation, again in contrast with our simulation, where the relevant branching ratio ranged between roughly 50% up to 100%. These two facets of the study, of course, enhance the signal-to-background ratio in the ATLAS study. Of course, there are further differences, like the missing underlying event in SHERPA, which

has been included in the ATLAS study, like slightly different selection cuts, like a different choice of PDF (CTEQ5L in ATLAS, CTEQ6L in our study) and, most importantly, like the inclusion of detector effects through their fast detector simulation ATLFAST [49] in the ATLAS study that are totally absent in our case. To summarize: However different in detail the studies are, it is reassuring to see that in all cases this seems to be a feasible channel, at least at accumulated higher luminosities.

In addition to the findings above, cf. Tables 3 and 4 we have identified two further distributions that may be worthwhile to study in the  $ZH$  channel:

- The total transverse momentum of the leptons and  $\cancel{p}_T$ , i.e. the total transverse momentum of the  $H$  and  $Z$  candidates (see Fig. 6). This observable shows a significantly different behaviour between the signals and the backgrounds, where the signal tends to be more strongly peaked towards small values.
- The azimuthal angle between  $\cancel{p}_T$  and the momentum of the lepton pair (see Fig. 7). Here the signal tends towards a more back-to-back configuration of the  $Z$  and  $H$  candidate. Seemingly, there is a significantly higher QCD activity in the backgrounds than in the signal, providing more jets for the  $ZH$ -candidate pair to recoil against in the backgrounds.

These findings may help to further improve the signal-to-background ratio.

## 4.2 Vector Boson Fusion

The other production channel we consider for invisibly decaying Higgs bosons at the LHC is vector boson fusion (VBF). As the name suggests, in this process the Higgs boson is produced through the fusion of two vector bosons emitted by quarks inside the protons, which typically carry comparably large momentum fractions of the protons. Therefore, at leading order (tree-level) there is no colour exchange between the two protons, and it can be expected that the central rapidity region remains to a large extent empty apart from the decay products of the produced system. The quarks on the other hand will be deflected, typically by transverse momenta of roughly half the mass of the produced system. This gives rise to two hard jets, which, due to the invisible nature of the Higgs boson, are essentially the triggers in this analysis. The main background processes to be taken into account are the production of  $Z$  or  $W$  bosons in association with two jets, which can originate either from QCD or through electroweak interactions, thus mimicking the topology of the VBF signal. In addition, top-pair production with subsequent semi-leptonic decays must be considered. Similar to the case of  $W$  production, the lepton is then

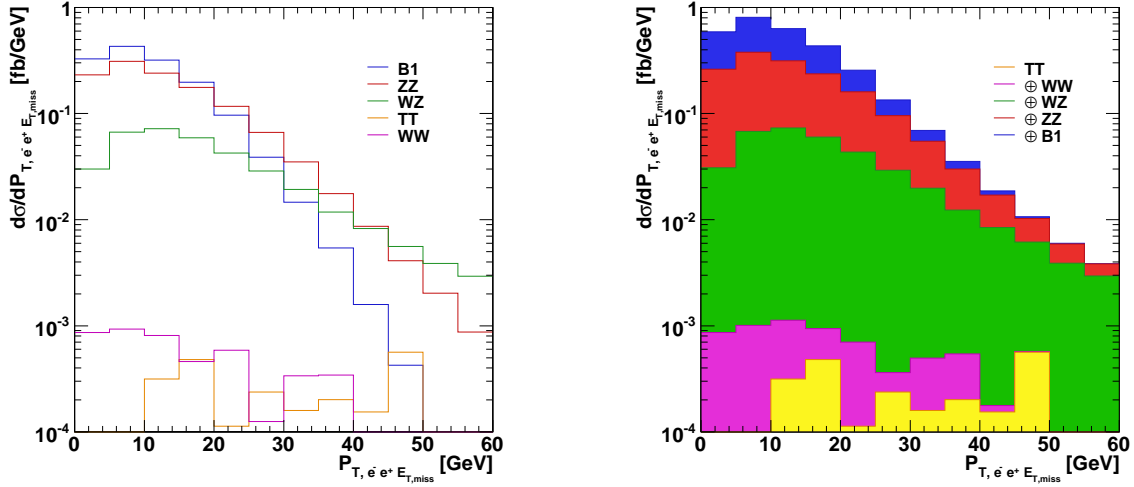


Figure 6: The  $p_T(e^+e^-, \cancel{E}_T)$  distribution for the signal in benchmark scenario B1 and the individual backgrounds. The left panel displays individual distributions while the right panel shows the sum of backgrounds and signal, starting from the lowest significant background.

lost. Again, it is worth noting that it should be possible to extract information concerning the total rates of these backgrounds, even after selection cuts, directly from data. This is possible either by reweighting leptonic  $Z$  decays to those into neutrino pairs, or, with a somewhat larger error, by extrapolating the modes where the individual lepton is seen (in  $W$ +jets or semileptonic top-pairs) into those regions where the lepton is lost. This is in analogy to the case discussed above. We employ the basic cuts listed in Ref. [29], i.e. we require :

1. two tagging jets with

- (a)  $p_{T,j} > 40 \text{ GeV}$ ,  $|\eta_j| < 5$ ,
- (b)  $|\eta_{j_1} - \eta_{j_2}| > 5$ ,  $\eta_{j_1} \cdot \eta_{j_2} < 0$ ,
- (c)  $m_{j_1 j_2} > 1700 \text{ GeV}$ ,
- (d)  $\Delta\phi_{j_1 j_2} = |\phi_{j_1} - \phi_{j_2}| < 1$ ,

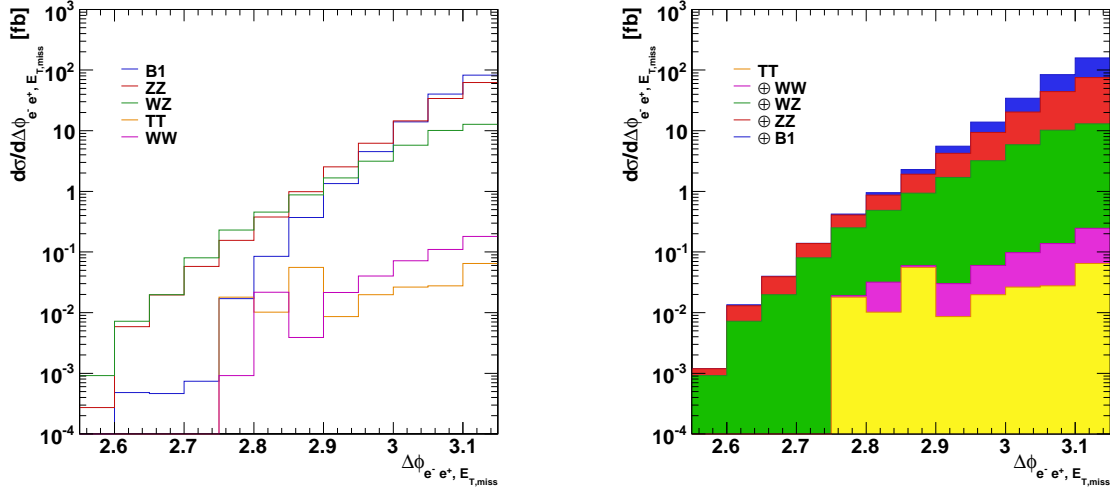


Figure 7: The  $\Delta\phi(e^+e^-, \cancel{E}_T)$  distribution for the signal in benchmark scenario B1 and backgrounds. The left panel displays individual distributions while the right panel shows the sum of backgrounds and signal, starting from the lowest significant background.

2. missing transverse momentum,  $\cancel{p}_T > 100$  GeV;

3. no identified lepton, i.e. no lepton with

$$(a) \ p_T^{e,\mu} > 5, 6 \text{ GeV in } |\eta_l| < 2.5,$$

4. a central jet veto, i.e. no jets with

$$p_T > 20 \text{ GeV, } \min\{\eta_{j_1}, \eta_{j_2}\} < \eta < \max\{\eta_{j_1}, \eta_{j_2}\}.$$

Additionally we impose :

$$5. \ |\eta_3^*| = \left| \eta_{j_3} - \frac{1}{2}(\eta_{j_1} + \eta_{j_2}) \right| > 1.5,$$

$$6. \ \Delta\phi_{j_1, j_3}, \ \Delta\phi_{j_2, j_3} < 1.25.$$

The choice of the cut on the invariant tagging jet mass of  $m_{jj} > 1700$  GeV is motivated by the corresponding invariant mass spectrum shown in Fig. 8. We observe that the signal distribution crosses the background at  $m_{jj} \approx 1700$  GeV. Of course this statement sensitively

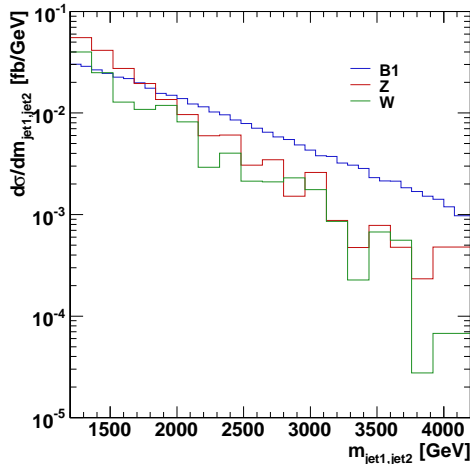


Figure 8: Tagjet invariant mass distribution for benchmark point B1 and the  $Z$  and  $W$  backgrounds.

depends on the model parameters chosen; however, the common feature of all scenarios is that the higher the invariant mass cut, the better the signal-to-background ratio. This is due to the fact that in a large fraction of background events the two tagging jets originate from QCD or the decay of weak gauge bosons.

After the above cuts the possibilities to check for the signal topology are limited in the VBF channel. Possible objects to be identified experimentally are the tagging jets,  $\not{p}_T$  and an eventually arising soft third jet. Therefore most observables show the same behaviour for signal and background, which is exemplified in the left panel of Fig. 9, showing the  $H_T$ -distribution for the signal at benchmark point B1 and the  $Z$  background. In the right panel of Fig. 9 we show for the same scenario the  $\eta_3^*$  distribution. It is clearly seen that for the background the third jet tends to be more central between the tagging jets, while for the signal it is rather forward or backward. This motivates the first of the additional cuts above.

For the various backgrounds listed above, cross sections before and after additional selection cuts, and the number of generated events are listed in Table 5. Signal cross sections before and after additional selection cuts are listed in Table 6. Putting together numbers, we again find appreciable signal-to-background ratios between more than 1/3

	$Z$ +jets (QCD+EW)	$W$ +jets (QCD+EW)	$t\bar{t}$
$\sigma_{\text{tot}}^{\text{gen}}$ [nb]	9.41	51.8	0.145
tagging jets	$1.80 \cdot 10^{-4}$	$7.44 \cdot 10^{-5}$	$1.62 \cdot 10^{-3}$
$m_{jj} > 1700$ GeV	$3.49 \cdot 10^{-5}$	$1.64 \cdot 10^{-5}$	$4.44 \cdot 10^{-4}$
$p_T > 100$ GeV	$2.64 \cdot 10^{-5}$	$9.73 \cdot 10^{-6}$	$3.32 \cdot 10^{-4}$
lepton veto	$2.63 \cdot 10^{-5}$	$2.84 \cdot 10^{-6}$	$1.28 \cdot 10^{-5}$
$\Delta\phi_{j_1 j_2} < 1$	$4.03 \cdot 10^{-6}$	$9.87 \cdot 10^{-7}$	$2.79 \cdot 10^{-5}$
central jet veto	$1.54 \cdot 10^{-6}$	$2.18 \cdot 10^{-7}$	$1.44 \cdot 10^{-6}$
$ \eta^*  > 1.5$	$1.37 \cdot 10^{-6}$	$1.95 \cdot 10^{-7}$	$6.70 \cdot 10^{-7}$
$\Delta\phi_{j_1 j_3}, \Delta\phi_{j_2 j_3}$	$1.14 \cdot 10^{-6}$	$1.44 \cdot 10^{-7}$	$4.29 \cdot 10^{-7}$
$\sigma_{\text{eff}}$ [fb]	10.7	7.45	0.0621

Table 5: Generation characteristics for the background processes to the VBF-channel. Here, the  $Z$  boson decays to neutrinos, whereas the  $W$  boson decays to any lepton–neutrino pair. For the top-pairs, semileptonic decays only have been considered.

	$B_1$	$B_2$	$B_3$	$B_4$	$B_5$
$\sigma_{\text{tot}}^{\text{gen}}$ [pb]	5.46	4.46	2.99	2.06	1.32
tagging jets	$4.38 \cdot 10^{-2}$	$5.59 \cdot 10^{-2}$	$6.80 \cdot 10^{-1}$	$7.54 \cdot 10^{-2}$	$8.12 \cdot 10^{-1}$
$m_{jj} > 1700$ GeV	$1.69 \cdot 10^{-2}$	$2.20 \cdot 10^{-2}$	$2.74 \cdot 10^{-2}$	$3.07 \cdot 10^{-2}$	$3.36 \cdot 10^{-2}$
$p_T > 100$ GeV	$1.46 \cdot 10^{-2}$	$1.90 \cdot 10^{-2}$	$2.37 \cdot 10^{-2}$	$2.67 \cdot 10^{-2}$	$2.92 \cdot 10^{-2}$
lepton veto	$1.46 \cdot 10^{-2}$	$1.90 \cdot 10^{-2}$	$2.37 \cdot 10^{-2}$	$2.66 \cdot 10^{-2}$	$2.92 \cdot 10^{-2}$
$\Delta\phi_{j_1 j_2} < 1$	$5.76 \cdot 10^{-3}$	$7.65 \cdot 10^{-3}$	$9.46 \cdot 10^{-3}$	$1.06 \cdot 10^{-2}$	$1.18 \cdot 10^{-2}$
central jet veto	$3.42 \cdot 10^{-3}$	$4.33 \cdot 10^{-3}$	$5.35 \cdot 10^{-3}$	$6.06 \cdot 10^{-3}$	$6.64 \cdot 10^{-3}$
$ \eta^*  > 1.5$	$3.40 \cdot 10^{-3}$	$4.31 \cdot 10^{-3}$	$5.32 \cdot 10^{-3}$	$6.03 \cdot 10^{-3}$	$6.60 \cdot 10^{-3}$
$\Delta\phi_{j_1 j_3}, \Delta\phi_{j_2 j_3}$	$3.11 \cdot 10^{-3}$	$3.92 \cdot 10^{-3}$	$4.81 \cdot 10^{-3}$	$5.45 \cdot 10^{-3}$	$5.97 \cdot 10^{-3}$
$\sigma_{\text{eff}}$ [fb]	17.0	17.5	14.4	11.2	7.9

Table 6: Generation characteristics for the signal processes in the VBF-channel, for the different benchmark scenarios.

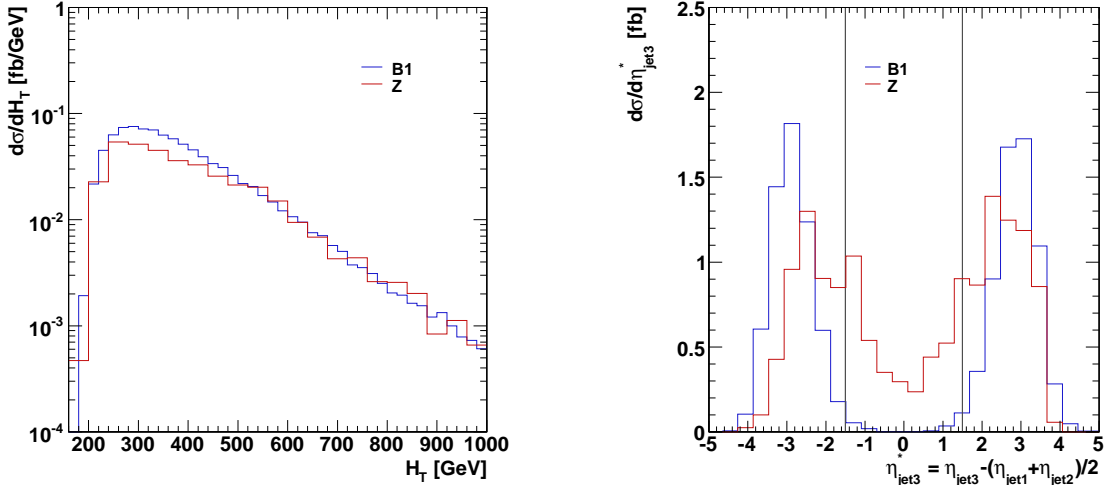


Figure 9: Left panel:  $H_T$  distribution for benchmark point B1 and  $Z$  background. Right panel:  $\eta_3^*$ - distribution for benchmark point B1 and  $Z$  background.

up to nearly 1 for all the benchmark points in the model. However, this finding has to be taken with more than a pinch of salt: first of all, similar to the  $ZH$  channel, we included all effects due to fragmentation, hadron decays, QED bremsstrahlung etc., and we typically added at least one further jet for a better modelling of additional hard QCD radiation. We did not, however, include the effects of the underlying event, which here could play a significant role in filling the rapidity gap between the two tagging jets, and thus lead to a corresponding reduction in the effective cross section after selection cuts. In addition we did not include diagrams where the Higgs boson is produced through an effective  $ggH$  coupling, mediated by heavy quarks. Although in principle the cross section for this mode is large, we note that previous work in the framework of the Standard Model suggests that the typical VBF cuts render this contribution insignificant [50–53]. Also, again, we did not simulate events at the detector-level which could further modify our findings.

However, again our results are in qualitative agreement with results of such a simulation at the detector level, which has been performed for the ATLAS experiment [29]. The results of this study were obtained using a fast detector simulation, and they are quite encouraging, too. Although in qualitative agreement, there are several differences: Again, the first one

lies in the choice of the event generator. ATLAS chose PYTHIA to compute both signal and SM backgrounds at leading order, while we employed SHERPA. In the ATLAS simulation SM coupling strength for the  $HVV$  couplings has been assumed with a 100% branching fraction of the Higgs decay to invisible, while in our study the  $HVV$  coupling is shielded through the mixing of the scalars, and the relevant branching ratio ranges between 0.5 and 1. While in ATLAS' PYTHIA simulation the effect of hard QCD radiation is typically accounted for by the parton shower, SHERPA uses exact matrix element, leading to a significantly increased jet activity. Also, SHERPA naturally includes spin correlations, and VBF-like background topologies are also taken care off, which have been missed in the ATLAS simulation. These effects, together, would typically reduce the signal-to-background ratio in our simulation with respect to the ATLAS study. On the other hand, the effect of the underlying event as well as the fast detector simulation, both included in the ATLAS analysis but ignored by us, may have the opposite implications on the visibility of the signal. Finally, it is worth stressing that we have also chosen different optimization cuts, in particular cuts 5 and 6, to enhance the signal over the background.

Nevertheless, to summarize, we again find that the prospects of finding an invisibly decaying Higgs boson at the LHC are much better than naively anticipated, and the two channels considered here may very well play a significant role in the phenomenology of non-standard scalar sectors.

## 5 Non-Abelian Phantom Sector

So far only a  $G_P = U(1)$  group theoretic phantom sector has been considered. The obvious question to be asked is how the Higgs boson observability will be affected in the case of non-Abelian extensions of the phantom sector (like  $G_P = SU(N)$ ). This will briefly be discussed in this section. As an overall result, in general, such extensions typically result in further suppression of the Higgs boson visible event rates,  $\mathcal{R}_i^2$ . Furthermore, in the case of more involved representations or multiple vector representations of  $G_P$  the “Higgs  $\rightarrow$  invisible” signal is decreased to a non-detectable rate. Some examples supporting this result will be presented in the following.

Consider for instance a  $G_P = SU(N)$  vector representation of scalar phantom fields,  $\vec{\Phi}$ . Then  $SU(N)$  is spontaneously broken down to  $SU(N-1)$  with  $2N-1$  physical NGBs and one physical SM-singlet scalar field that eventually mixes with the  $SU(2)_L$  Higgs field. It is a textbook exercise to prove that eq. (1.5) in such a framework becomes

$$\mathcal{L}_{\text{int}} = -\frac{m_{H_i}^2}{2\sigma} O_{i2} H_i(x) \mathcal{J}^a(x) \mathcal{J}^a(x) \quad \text{with } a = 1 \dots (2N-1). \quad (5.8)$$

This suggests that the Higgs boson decay width broadens compared to the  $G_P = U(1)$  case. The visible Higgs boson event rates (there are still two physical states) read

$$\mathcal{R}_1^2 \simeq \left[ (1 + \tan^2 \theta) \left( 1 + \frac{2N-1}{12} \frac{m_{H_1}^2}{m_b^2} \tan^2 \theta \tan^2 \beta \right) \right]^{-1},$$

$$\mathcal{R}_2^2 \simeq \left[ (1 + \cot^2 \theta) \left( 1 + \frac{2N-1}{12} \frac{m_{H_2}^2}{m_b^2} \cot^2 \theta \tan^2 \beta \right) \right]^{-1}.$$

Hence increasing the rank of the phantom gauge group results in a ( $1/N$  for large  $N$ ) decrease in visible Higgs boson rates. Searching for “Higgs  $\rightarrow$  invisible” is therefore vital. Note also that increasing the rank of the phantom symmetry group does not necessarily imply different “Higgs  $\rightarrow$  invisible” rates. In fact, in the above example we still have two physical scalars in the spectrum for which the equation  $\mathcal{T}_1 + \mathcal{T}_2 \approx 1$  is valid, similarly to the  $G_P = U(1)$  case.

It may also be the case that additional physical Higgs bosons fragment the “Higgs  $\rightarrow$  invisible” rate into many small pieces such that any detection at the LHC seems completely impossible. This case can be illustrated with the following example: consider  $G_P = SU(3)$  broken by 2 sets of vector representations down to the null group. We start with 12 degrees of freedom, out of which 8 become NGBs and the other 4 become massive scalar fields. These 4 fields will mix with the one  $SU(2)_L$  Higgs field through the  $(5 \times 5)$  matrix  $O$  forming 5 physical Higgs-boson eigenstates. In this case, due to the unitarity of the matrix  $O$  we have  $\sum_{i=1}^5 \mathcal{T}_i^2 \approx 1$ , which allows for  $\mathcal{T}_i^2 \lesssim 0.25$ . Such a “Higgs  $\rightarrow$  invisible” rate is most probably beyond reach of discovery (or exclusion) at the LHC [27, 29] - a truly nightmarish scenario!

## 6 Additional Remarks

It should be emphasized that in the scenario considered in this article, invisible Higgs boson phenomenology, small neutrino masses and the correct baryon asymmetry (see also ref. [13]) are all obtained without fine-tuning coupling constants. All scalars have masses at the EW scale ( $\tan \beta \approx 1$ ) and so there are no ultra-heavy scalars to destabilize this hierarchy. However, the model does not include gravity nor does it contain a mechanism or theoretical explanation as to why  $\sigma \ll M_{\text{Planck}}$ . Although the SM hierarchy problem is not solved in this model the question here is somewhat different: *Why is the phantom sector symmetry broken at the EW scale?* We cannot provide a non-common (*i.e.*, non-supersymmetric) answer to this question, and refer to [54, 55].

Instead of a theory with one global symmetry, one could imagine a theory where several symmetries were gauged (or left un-gauged), absorbing the NGBs into massive gauge bosons through the Higgs mechanism. This is an absolutely viable option, although the requirement of anomaly cancellation would result in model dependencies. Such models have been proposed before and studied in some detail in the recent literature [56]. Generally speaking, these models lead to phenomenology that includes the (observable) decays of the extra gauge bosons, with all constraints on their masses etc..

Recently there has been renewed interest in the possibilities offered by extending the Standard Model with a real scalar singlet [57]. Depending on the symmetries of the model it is possible to provide a candidate for the cold dark matter in the universe (extra discrete symmetries needed) [58], and it is possible to provide a strong first-order electroweak phase transition suitable for electroweak baryogenesis [59]. It should be noted in the latter case that an additional source of CP-violation would be necessary to provide a complete mechanism for baryogenesis.

Models with broken discrete symmetries provide another possible way of avoiding invisible decays of Higgs boson(s). Clearly, spontaneous breaking of such symmetries does not lead to NGBs, making the Higgs boson signatures more visible. There are, however, so many possibilities of such groups that a particular choice renders this idea less appealing and convincing. Spontaneously broken discrete symmetries may also, in some cases, produce unwanted cosmological relics such as domain-walls, potentially placing severe constraints on this class of model.

## 7 Conclusions

Physical NGBs arise when continuous global symmetries are spontaneously broken. Such broken symmetries may be related to the smallness of neutrino masses or the patterns of mixing angles (in the case of familons). In this article we show that the role of NGBs in Higgs boson phenomenology is very important; they lead to the dilution and potential invisibility of the expected SM signal. Working with approximate analytic formulae we first identified regions of parameter space [eq. (1.6)] where Higgs boson phenomenology is challenging both for past LEP data and for the future LHC experiments, and secondly implemented the model in SHERPA, ready for further analysis by experimenters when real LHC data arrive.

Our study shows that LEP excludes the minimal phantom sector case where both Higgs bosons have masses  $m_H \lesssim 85$  GeV irrespective of their decay modes. However,

experimentally allowed scenarios exist where one Higgs boson mass is much lower than the SM Higgs boson exclusion limit,  $m_{H_1} = 68$  GeV, and the other is just at this limit,  $m_{H_2} = 114$  GeV.

In light of the nightmarish potential of this scenario, Monte-Carlo simulation studies of invisible Higgs boson searches at the LHC are performed. Two search channels are looked at in detail; the associated production of a  $Z$  and a Higgs boson, and the production of a Higgs boson in weak vector boson fusion. For  $ZH$  associated production, it is found that in each of 5 benchmark scenarios, the invisible Higgs boson should be found at the LHC, with signal-to-background ratios of order  $S/B \simeq 1/8$  to 1. Scope for improving this ratio is also found by looking either at the distribution of the total transverse momentum of the leptons and the  $\cancel{p}_T$ , or at the distribution of the azimuthal angle between the  $\cancel{p}_T$  and the momentum of the lepton pair. Fairly good signal-to-background ratios are also found in the vector boson fusion search channel. However in this case the effects of the underlying event, which was not included in simulations, may reduce the amount of signal passing the selection cuts.

Although our MC analysis focuses on the case with an Abelian phantom sector symmetry, we also examined cases with non-Abelian symmetries in the phantom sector using the analytic formulae provided in section 3. For the case  $G_P = SU(N)$  we found that the visibility of the Higgs bosons is reduced when we increase the rank of the  $SU(N)$  group making the LHC searches to invisible a necessity. In addition, by choosing appropriate representations of the group for breaking the symmetry we may further dilute the Higgs boson to invisible signature, leading to a very difficult scenario indeed for the LHC.

Regarding the hierarchy problem, the model at hand is not better or worse than the Standard Model. Any difference could be interpreted as shifting the problem to the phantom sector which sets the scale of the symmetry breaking.

## Acknowledgements

We would like to thank Karl Jacobs for letting us know about progress on ATLAS studies of Higgs to invisible. A.D. would like to thank the European Artemis network and especially Nikos Konstantinidis for discussions on “Higgs to invisible” at LEP. We are all fully (S.H.) or partially supported by the RTN European Programme, MRTN-CT-2006-035505 (HEPTOOLS, Tools and Precision Calculations for Physics Discoveries at Colliders) or by the RTN European Programme MRTN-CT-2006-035606 (MCnet).

## Appendix A $U(1)$ Phantom Model Feynman Rules

In this appendix we present Feynman rules for the Higgs sector of  $G_{SM} \times \{G_P = U(1)_P\}$  that are relevant for Higgs phenomenology at LEP and the LHC. Feynman rules for the trilinear couplings  $H_i \mathcal{J} \mathcal{J}$ ,  $H_1 H_2 H_i$ ,  $H_i H_i H_i$ ,  $W^+ W^- H_i$ ,  $ZZ H_i$ , and  $f \bar{f} H_i$  for  $i = 1, 2$  are shown in Fig. 10. For completeness in Fig. 11, also Feynman rules for the quadrilinear couplings  $H_i H_j \mathcal{J} \mathcal{J}$ ,  $H_i H_j H_k H_l$ ,  $H_i H_j ZZ$ , and  $H_i H_j W^+ W^-$  are listed.

$M_W$  and  $M_Z$  are the masses of the  $W$  boson and  $Z$  boson, respectively and  $m_f$  is the fermion mass which can be either a quark or a lepton. The  $SU(2)_L$  coupling constant is  $g_2$  and  $\theta_w$  is the Weinberg mixing angle.  $v$  is the vacuum expectation value for the standard model  $SU(2)_L$  Higgs doublet  $H$ .  $g_{\mu\nu}$  is the Minkowski spacetime metric  $(1, -1, -1, -1)$ .

The orthogonal mixing matrix,  $O$ , is

$$O = \begin{pmatrix} O_{11} & O_{12} \\ O_{21} & O_{22} \end{pmatrix} = \begin{pmatrix} \cos \theta & \sin \theta \\ -\sin \theta & \cos \theta \end{pmatrix}. \quad (\text{A.1})$$

Here  $\tan \beta = v/\sigma$  with  $\sigma \equiv \langle \Phi \rangle$ .  $m_{H_1}$  and  $m_{H_2}$  denote the masses of the two Higgs bosons,  $H_1$  and  $H_2$ , respectively.

$$: -i \frac{m_f}{v} O_{i1}$$

$$: i \frac{g_2 M_Z}{\cos \theta_w} O_{i1} g_{\mu\nu}$$

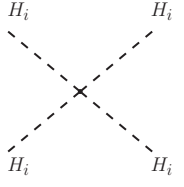
$$: i g_2 M_W O_{i1} g_{\mu\nu}$$

$$: -i \frac{m_{H_i}^2}{v} \tan \beta O_{i2}$$

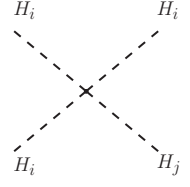
$$: \frac{i}{v} (m_{H_1}^2 + m_{H_2}^2 + m_{H_i}^2) \cdot O_{i1} O_{i2} (O_{1i} + O_{2i} \tan \beta)$$

$$: -3i \frac{m_{H_i}^2}{v} (O_{i1}^3 + O_{i2}^3 \tan \beta)$$

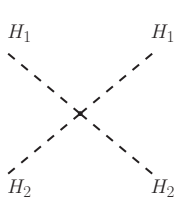
Figure 10: *Trilinear couplings.*



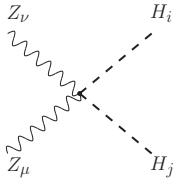
$$\begin{aligned}
& : & - \frac{3i}{v^2} [O_{1i}^4 (m_{H_1}^2 O_{11}^2 + m_{H_2}^2 O_{12}^2) \\
& & + O_{i2}^4 (m_{H_2}^2 O_{11}^2 + m_{H_2}^2 O_{12}^2) \tan^2 \beta \\
& & - 2O_{12}^3 O_{11}^3 \tan \beta (m_{H_2}^2 - m_{H_1}^2)]
\end{aligned}$$



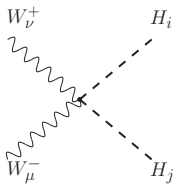
$$\begin{aligned}
& : & + \frac{3i}{v^2} O_{11} O_{ij} (O_{j2} + O_{j1} \tan \beta) \\
& & \cdot [m_{H_i}^2 (O_{i2}^3 \tan \beta + O_{i1}^3) \\
& & + m_{H_j}^2 (O_{i1} O_{j1}^2 + O_{i2} O_{j2}^2 \tan \beta)] \\
& (i \neq j)
\end{aligned}$$



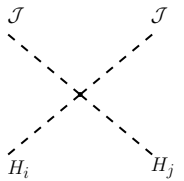
$$\begin{aligned}
& : & + \frac{i}{v^2} O_{11} O_{12} [(m_{H_2}^2 - m_{H_1}^2) \tan \beta \\
& & \cdot (O_{11}^4 - 4O_{12}^2 O_{11}^2 + O_{12}^4) \\
& & + 3O_{11} O_{12} (m_{H_1}^2 O_{11}^2 + m_{H_2}^2 O_{12}^2 \\
& & + (m_{H_2}^2 O_{11}^2 + m_{H_1}^2 O_{12}^2) \tan^2 \beta)]
\end{aligned}$$



$$: \frac{ig_2^2}{2} g_{\mu\nu} O_{i1} O_{j1}$$



$$: \frac{ig_2^2}{2 \cos^2 \theta_w} g_{\mu\nu} O_{i1} O_{j1}$$



$$\begin{aligned}
& : & + \frac{i}{v^2} [-O_{i2} O_{j2} (m_{H_1}^2 O_{12}^2 + m_{H_2}^2 O_{11}^2) \tan^2 \beta \\
& & + (m_{H_2}^2 - m_{H_1}^2) O_{12} O_{11} O_{i1} O_{j1} \tan \beta]
\end{aligned}$$

Figure 11: *Quadrilinear couplings.*

## References

- [1] J. Goldstone, A. Salam and S. Weinberg, Phys. Rev. **127**, 965 (1962).
- [2] J. Goldstone, Nuovo Cim. **19** (1961) 154.
- [3] Y. Nambu, Phys. Rev. Lett. **4**, 380 (1960).
- [4] R. E. Shrock and M. Suzuki, Phys. Lett. B **110**, 250 (1982). For later studies, see also, L. F. Li, Y. Liu and L. Wolfenstein, Phys. Lett. B **159**, 45 (1985); G. Jungman and M. A. Luty, Nucl. Phys. B **361** (1991) 24; A. S. Joshipura and S. D. Rindani, Phys. Rev. Lett. **69** (1992) 3269; A. S. Joshipura and J. W. F. Valle, Nucl. Phys. B **397** (1993) 105.
- [5] S. Weinberg, Phys. Rev. Lett. **40**, 223 (1978); F. Wilczek, Phys. Rev. Lett. **40**, 279 (1978).
- [6] F. Wilczek, Phys. Rev. Lett. **49**, 1549 (1982).
- [7] Y. Chikashige, R. N. Mohapatra and R. D. Peccei, Phys. Lett. B **98**, 265 (1981); G. B. Gelmini and M. Roncadelli, Phys. Lett. B **99**, 411 (1981).
- [8] R. D. Peccei and H. R. Quinn, Phys. Rev. D **16**, 1791 (1977); Phys. Rev. Lett. **38**, 1440 (1977).
- [9] W-M Yao et al 2006 J. Phys. G: Nucl. Part. Phys. **33** 1232 .
- [10] A. Pilaftsis, arXiv:0805.1677 [hep-ph].
- [11] P. Minkowski, Phys. Lett. B **67** (1977) 421;  
M. Gell-Mann, P. Ramond and R. Slansky, in *Supergravity*, eds. D.Z. Freedman and P. van Nieuwenhuizen (North-Holland, Amsterdam, 1979);  
T. Yanagida, in Proc. of the *Workshop on the Unified Theory and the Baryon Number in the Universe*, Tsukuba, Japan, 1979, eds. O. Sawada and A. Sugamoto;  
R. N. Mohapatra and G. Senjanović, Phys. Rev. Lett. **44** (1980) 912.
- [12] M. Roncadelli and D. Wyler, Phys. Lett. B **133** (1983) 325.
- [13] D. G. Cerdeno, A. Dedes and T. E. J. Underwood, JHEP **0609** (2006) 067.
- [14] K. Dick, M. Lindner, M. Ratz and D. Wright, Phys. Rev. Lett. **84** (2000) 4039. See also, H. Murayama and A. Pierce, Phys. Rev. Lett. **89** (2002) 271601; B. Thomas

- and M. Toharia, Phys. Rev. D **73** (2006) 063512; Phys. Rev. D **75**, 013013 (2007) [arXiv:hep-ph/0607285]; B. Thomas, arXiv:0712.4134 [hep-ph]; E. J. Chun and P. Roy, JHEP **0806**, 089 (2008) [arXiv:0803.1720 [hep-ph]].
- [15] P. H. Gu and H. J. He, JCAP **0612** (2006) 010 [arXiv:hep-ph/0610275]; P. H. Gu, H. J. He and U. Sarkar, JCAP **0711** (2007) 016 [arXiv:0705.3736 [hep-ph]]; Phys. Lett. B **659** (2008) 634 [arXiv:0709.1019 [hep-ph]]; P. H. Gu and U. Sarkar, Phys. Rev. D **77** (2008) 105031 [arXiv:0712.2933 [hep-ph]].
- [16] R. N. Mohapatra and P. B. Pal, “*Massive neutrinos in physics and astrophysics*. Second edition,” World Sci. Lect. Notes Phys. **60**, 1 (1998) [World Sci. Lect. Notes Phys. **72**, 1 (2004)].
- [17] B. Patt and F. Wilczek, arXiv:hep-ph/0605188. Singlet extensions of the Higgs sector of the SM have been considered previously in e.g., J. J. van der Bij, Phys. Lett. B **636**, 56 (2006) [arXiv:hep-ph/0603082] and references therein. See also T. Binoth and J. J. van der Bij, Z. Phys. C **75** (1997) 17 [arXiv:hep-ph/9608245].
- [18] S. R. Coleman and E. Weinberg, Phys. Rev. D **7** (1973) 1888.
- [19] J. R. Espinosa and M. Quiros, Phys. Rev. D **76** (2007) 076004 [arXiv:hep-ph/0701145]; W. F. Chang, J. N. Ng and J. M. S. Wu, Phys. Rev. D **75** (2007) 115016 [arXiv:hep-ph/0701254].
- [20] [LEP Higgs Working for Higgs boson searches Collaboration], “Searches for invisible Higgs bosons: Preliminary combined results using LEP data collected at energies up to 209-GeV,” arXiv:hep-ex/0107032.
- [21] F. de Campos, O. J. P. Eboli, J. Rosiek and J. W. F. Valle, Phys. Rev. D **55**, 1316 (1997) [arXiv:hep-ph/9601269].
- [22] S. P. Martin and J. D. Wells, Phys. Rev. D **60**, 035006 (1999) [arXiv:hep-ph/9903259].
- [23] H. Davoudiasl, T. Han and H. E. Logan, Phys. Rev. D **71** (2005) 115007 [arXiv:hep-ph/0412269].
- [24] S. G. Frederiksen, N. Johnson, G. L. Kane and J. Reid, Phys. Rev. D **50** (1994) 4244.
- [25] R. M. Godbole, M. Guchait, K. Mazumdar, S. Moretti and D. P. Roy, Phys. Lett. B **571** (2003) 184 [arXiv:hep-ph/0304137].
- [26] K. Jacobs, *private communication*.

- [27] F. Meisel, M. Dürrssen, M. Heldmann, K. Jacobs, ATL-PHYS-PUB-2006-009.
- [28] O. J. P. Eboli and D. Zeppenfeld, Phys. Lett. B **495** (2000) 147 [arXiv:hep-ph/0009158].
- [29] L. Neukermans, B. Di Girolamo, ATL-PHYS-2003-006.
- [30] K. Belotsky, V. A. Khoze, A. D. Martin and M. G. Ryskin, Eur. Phys. J. C **36**, 503 (2004) [arXiv:hep-ph/0406037].
- [31] For a review see, M. Sher, Phys. Rept. **179**, 273 (1989). In particular see, M. Sher, Phys. Lett. B **317**, 159 (1993) [Addendum-ibid. B **331**, 448 (1994)] [arXiv:hep-ph/9307342]; T. Hambye and K. Riesselmann, Phys. Rev. D **55**, 7255 (1997) [arXiv:hep-ph/9610272]; C. F. Kolda and H. Murayama, JHEP **0007**, 035 (2000) [arXiv:hep-ph/0003170].
- [32] M. E. Machacek and M. T. Vaughn, Nucl. Phys. B **249**, 70 (1985).
- [33] M. Bowen, Y. Cui and J. D. Wells, JHEP **0703**, 036 (2007) [arXiv:hep-ph/0701035].
- [34] In addition to ref. [31], see also J. F. Gunion, H. E. Haber, G. L. Kane and S. Dawson, “The Higgs Hunter’s Guide” , Frontiers in Physics, p.64. and, H. Arason, D. J. Castano, B. Keszthelyi, S. Mikaelian, E. J. Piard, P. Ramond and B. D. Wright, Phys. Rev. D **46**, 3945 (1992).
- [35] S. Schael *et al.* [ALEPH Collaboration], Eur. Phys. J. C **47**, 547 (2006) [arXiv:hep-ex/0602042].
- [36] In all exclusion plots we use, R. Barate *et al.* [ALEPH Collaboration], Phys. Lett. B **466**, 50 (1999); Phys. Lett. B **450**, 301 (1999); M. Acciarri *et al.* [L3 Collaboration], Phys. Lett. B **485**, 85 (2000) [arXiv:hep-ex/0004006]; [LEP Higgs Working for Higgs boson searches Collaboration], arXiv:hep-ex/0107032; G. Abbiendi [OPAL Collaboration], arXiv:0707.0373 [hep-ex].
- [37] G. Abbiendi *et al.* [OPAL Collaboration], Eur. Phys. J. C **18** (2001) 425 [arXiv:hep-ex/0007040].
- [38] R. Schabinger and J. D. Wells, Phys. Rev. D **72**, 093007 (2005) [arXiv:hep-ph/0509209].
- [39] R. Barate *et al.* [LEP Working Group for Higgs boson searches], Phys. Lett. B **565** (2003) 61 [arXiv:hep-ex/0306033].

- [40] O. Bahat-Treidel, Y. Grossman and Y. Rozen, arXiv:hep-ph/0611162.
- [41] See for instance, Fig. 7 from F. Gianotti and M. L. Mangano, arXiv:hep-ph/0504221. In addition, S. Bolognesi, “Higgs at CMS with 1, 10, 30 fb<sup>-1</sup>”, talk given at LCWS’07; R. Nikolaidou, “Higgs searches in ATLAS at low luminosity phase ( $\mathcal{L}$  up to 30 fb<sup>-1</sup>).
- [42] C. H. Shepherd-Themistocleous, *private communication*.
- [43] T. Gleisberg, S. Hoche, F. Krauss, A. Schalicke, S. Schumann and J. C. Winter, JHEP **0402** (2004) 056 [arXiv:hep-ph/0311263].
- [44] S. Catani, F. Krauss, R. Kuhn and B. R. Webber, JHEP **0111** (2001) 063 [arXiv:hep-ph/0109231].
- [45] J. Pumplin, D. R. Stump, J. Huston, H. L. Lai, P. Nadolsky and W. K. Tung, JHEP **0207** (2002) 012 [arXiv:hep-ph/0201195].
- [46] S. Catani, Y. L. Dokshitzer, M. Olsson, G. Turnock and B. R. Webber, Phys. Lett. B **269**, 432 (1991); S. Catani, Y. L. Dokshitzer and B. R. Webber, Phys. Lett. B **285**, 291 (1992); S. Catani, Y. L. Dokshitzer, M. H. Seymour and B. R. Webber, Nucl. Phys. B **406**, 187 (1993).
- [47] T. Sjostrand, Comput. Phys. Commun. **82** (1994) 74; T. Sjostrand, P. Eden, C. Friberg, L. Lonnblad, G. Miu, S. Mrenna and E. Norrbin, Comput. Phys. Commun. **135** (2001) 238 [arXiv:hep-ph/0010017].
- [48] M. Spira, *h2hv program*, <http://people.web.psi.ch/spira/v2hv/>
- [49] E. Richer-Was, D. Froidevaux and L. Poggioli, *ATLFAST, a fast simulation package for ATLAS*, ATLAS note, ATL-PHYS-98-131.
- [50] V. Del Duca, W. Kilgore, C. Oleari, C. Schmidt and D. Zeppenfeld, Nucl. Phys. B **616** (2001) 367 [arXiv:hep-ph/0108030].
- [51] V. Del Duca, W. Kilgore, C. Oleari, C. Schmidt and D. Zeppenfeld, Phys. Rev. Lett. **87** (2001) 122001 [arXiv:hep-ph/0105129].
- [52] J. R. Andersen, T. Binoth, G. Heinrich and J. M. Smillie, JHEP **0802** (2008) 057 [arXiv:0709.3513 [hep-ph]].
- [53] A. Bredenstein, K. Hagiwara and B. Jager, Phys. Rev. D **77** (2008) 073004 [arXiv:0801.4231 [hep-ph]].

- [54] F. Wilczek, arXiv:0708.4236 [hep-ph].
- [55] T. Hur, D. W. Jung, P. Ko and J. Y. Lee, arXiv:0709.1218 [hep-ph].
- [56] E. H. de Groot, G. J. Gounaris and D. Schildknecht, Phys. Lett. B **85**, 399 (1979); Z. Phys. C **5** (1980) 127; R. N. Mohapatra and R. E. Marshak, Phys. Rev. Lett. **44**, 1316 (1980) [Erratum-ibid. **44**, 1643 (1980)] and later references to this article. For a recent attempt to study LHC phenomenology in a gauged  $U(1)_{B-L}$  model, see, W. Emam and S. Khalil, arXiv:0704.1395 [hep-ph]; M. Abbas and S. Khalil, arXiv:0707.0841 [hep-ph].
- [57] M. C. Bento, O. Bertolami, R. Rosenfeld and L. Teodoro, Phys. Rev. D **62** (2000) 041302 [arXiv:astro-ph/0003350]; C. P. Burgess, M. Pospelov and T. ter Veldhuis, Nucl. Phys. B **619** (2001) 709 [arXiv:hep-ph/0011335]; H. Davoudiasl, R. Kitano, T. Li and H. Murayama, Phys. Lett. B **609** (2005) 117 [arXiv:hep-ph/0405097]; V. Barger, P. Langacker, M. McCaskey, M. J. Ramsey-Musolf and G. Shaughnessy, arXiv:0706.4311 [hep-ph].
- [58] J. McDonald, Phys. Rev. D **50**, 3637 (1994).
- [59] J. R. Espinosa and M. Quiros, in [19].